npj | regenerative medicine

Article

Published in partnership with the Australian Regenerative Medicine Institute

https://doi.org/10.1038/s41536-025-00409-y

Scale up manufacturing approach for production of human induced pluripotent stem cell-derived islets using Vertical Wheel® bioreactors

Nidheesh Dadheech[1,2,3] ✉, Mario Bermúdez de León[4,9], Zofia Czarnecka[1,2,9], Nerea Cuesta-Gomez[1,2], Ila Tewari Jasra[1,2], Rena Pawlick[1,2,3], Braulio Marfil-Garza[1,2,5], Sandhya Sapkota[1,2], Kevin Verhoeff[1,2], Haide Razavy[1,2], Perveen Anwar[1], Abhineet Singh[6], Nilanjan Ray[6], Doug O' Gorman[3], Glen Jickling[7], James Lyon[1], Patrick MacDonald[1,8] & A. M. James Shapiro[1,2,3] ✉

Advanced protocols show potential for human stem cells (SC)-derived islets generation under planar (2D) alone or three-dimensional (3D) cultures, but show challenges in scalability, cell loss, and batch-to-batch consistency. This study explores Vertical Wheel (VW)® bioreactor suspension technology to differentiate islets from human induced pluripotent stem cells, achieving uniform, transcriptionally mature, and functional SC-islets. A 5x increase in scale from 0.1 L to 0.5 L reactors resulted in a 12-fold (15,005–183,002) increase in islet equivalent count (IEQ) without compromising islet structure. SC-islets show enriched β-cell composition (~63% CPPT$^+$NKX6.1$^+$ISL1$^+$), glucose responsive insulin release (3.9–6.1-fold increase), and reversed diabetes in STZ-treated mice. Single cell RNA sequencing and flowcytometry analysis confirmed transcriptional maturity and functional identity, similar to adult islets. Lastly, harvested SC-islet grafts demonstrate improved islet functionality and mature transcriptomic signatures. Overall, scale-up in VW® bioreactor technology enhances IEQ yield with minimal variability and reduced cell loss, offering a pathway for clinical-grade SC-islet production.

Human islets derived from stem cells (SC) hold immense promise for the transformation of care for people living with diabetes[1–3]. The ability to generate large numbers of insulin-producing cells from human pluripotent SC can restore normal endogenous insulin production and effectively manage diabetes in both animal models[4,5] and human patients[6–10]. Recent advances in SC- islet manufacture have generated considerable clinical interest[11–16]. The ground-breaking application of this concept in human subjects was demonstrated by Vertex Pharmaceuticals, USA, in their clinical trial (NCT04786262). In this trial, embryonic stem cell (ESC)-derived islets (VX-880) were implanted into patients with type 1 diabetes (T1D). Intra-portal infusion of VX-880 cells resulted in 3 of 14 T1D patients becoming insulin independent with restoration of insulin secretion and glucose control[9]. Furthermore, ViaCyte Inc., USA (formerly Cythera, then Novocell and later acquired by Vertex), conducted two additional clinical trials (NCT02239354; NCT03163511) involving human ESC-derived pancreatic progenitor cells (VC01 and VC02) in T1D patients. These multicentric trials demonstrated safety of the cell product, histologic evidence of C-peptide cell survival and detection of relatively small amounts of C-peptide (above 50 ng/mL) in serum, but with only modest impact upon glycemic control[8,17]. Recently, Deng et al. showed success in using autologous induced pluripotent stem cell (iPSC)-derived islets in treating Type 1 Diabetes with reduced insulin requirements and safety profile at 1 year after transplant. Similarly, Wu et al. transplanted iPSC-derived islets intra-hepatically demonstrating the efficacy of these cell-products in also treating Type 2 Diabetes[10,18].

[1]Alberta Diabetes Institute, University of Alberta, Edmonton, AB, Canada. [2]Department of Surgery, University of Alberta, Edmonton, AB, Canada. [3]Clinical Islet Transplant Program, University of Alberta, Edmonton, AB, Canada. [4]Centro de Investigación Biomédica del Noreste, Departamento de Biología Molecular, Instituto Mexicano del Seguro Social, Monterrey, Nuevo León, Mexico. [5]CHRISTUS–LatAm Hub—Excellence and Innovation Center, Monterrey, Mexico. [6]Department of Computing Science, University of Alberta, Edmonton, AB, Canada. [7]Department of Medicine, University of Alberta, Edmonton, AB, Canada. [8]Department of Pharmacology, University of Alberta, Edmonton, AB, Canada. [9]These authors contributed equally: Mario Bermúdez de León, Zofia Czarnecka.
✉e-mail: dadheech@ualberta.ca; jshapiro@ualberta.ca

Transplantation of human cadaveric islets has been shown to be highly effective for patients with T1D complicated by labile glycemic control, and 20-year outcomes from the Edmonton Protocol and other variants continue to show promise[19]. Major drawbacks of this cell-based approach have been the need for risky life-long immunosuppression, and the limited supply of tissues from organ donors. Human ESC-derived islet-like progenitors could potentially address cell supply, but chronic immunosuppression, micro or macroencapsulation immune shielding or complex immune-target gene edits are required to overcome a need chronic immunosuppression[20]. Moreover, ESC-derived products continue to raise ethical concerns, and will likely not be acceptable to Catholic and other religious groups. Human iPSC may offer a more ethically favorable alternative. The discovery of iPSCs has provided an opportunity to reprogram adult somatic cells to a state of embryonic-like pluripotency, enabling the production of differentiated cell products without the need to destroy human embryos[21]. Additionally, generating SC-islets from a patient's own iPSCs could potentially enable autologous islet cell transplantation without need for chronic immunosuppression, at least in non-autoimmune diabetes populations[7].

Recent advancements in the generation of insulin-producing islet cells from human pluripotent stem cells (PSCs) show promising potential for cell-based therapy. Various research groups have successfully differentiated human PSCs into 3D endoderm[21,22], pancreatic progenitors[16,23,24], and mature SC-islets in suspension cultures using multi-well plates, flasks, or dishes[15,25–27] and spinner flasks[14,28–30]. Additionally, 2D planar differentiation[11,26,28,29] have been employed, where initial differentiation occurs in planar conditions up till pancreatic progenitor stage (Stage 4, S4). Subsequently, cell clusters are aggregated and transferred into 3D suspension culture using either ultra-low attachment plates[10] or AggreWell™ plates[11]. Challenges persist with these approaches however, including limitations in scale up, and risk of off-target cell populations that could compromise product safety[15].

Several techniques have emerged for differentiating human iPSC into islet-like organoids that closely mimic primary adult donor islets[7,9,16,23,26,27]. Recent studies have shown promise in enhancing maturation of SC-islets during in vitro differentiation. These improvements involve modifying culture conditions and incorporating serial small molecule growth factors or inhibitors to promote the metabolic and transcriptional maturity of islet cells[26,28–30]. Barsby et al.[63] was able to generate 8000–10,000 clusters per batch from pooled pancreatic progenitors using the protocol outlined by Balboa et al.[12]. Similarly, Hogrebe et al. reported the generation of 340–750 million S6 cells from 6 to 13 standard T-75 flasks, employing a method that requires pooling from multiple culture vessels[11]. Despite the potential for scale up using these approaches, unwanted batch-to-batch variability remains a concern, necessitating extensive manual cell processing, and risk of cellular off-target heterogeneity, ultimately rendering the process unreliable and costly.

A number of technologies have become available for scaling up SC-islet protocols, including CellFactory™, CellCube®, HYPERFlasks®, and multi-layered CellSTACKS® chambers[31]. It is estimated that for clinical application, patients will require at least 7000 to 12,000 islet equivalent counts (IEQ) per kilogram of body weight to achieve full reversal of diabetes[32]. A greater mass still will be required to restore normal metabolic profiles and provide glycemic reserve similar to a normal human pancreas. Based on these requirements, approximately a billion SC-derived islet cells would be necessary to attain glycemic control and insulin independence[26]. This target cell mass is currently beyond reach of existing planar or suspension platforms. While several groups have successfully produced high-quality islet cell products, scaling up these protocols and manufacturing them in single large batches with consistently reliable SC-islets remains a potential limitation[33]. Additionally, substantial cell loss occurs during the terminal stages of islet differentiation, with risk of unwanted off-target cells and cellular heterogeneity in the final product[26,31]. Purification steps including physical disaggregation-reaggregation is associated with substantial cell loss[32]. Stock et al. observed extensive cell loss up to 8 days post reaggregation, resulting in a total yield of ~21%[33]. Similarly, Veres et al. reported a recovery rate of only 6-10% of the final product post-sorting with Cd49a, a surface marker for SC-β cells[14].

Despite these scaling technologies, SC-islets still exhibit cellular heterogeneity and risk of off-target cell populations[34–37]. One potential solution is utilization of suspension culture bioreactors, such as Vertical-Wheel® bioreactors. Suspension bioreactors offer capacity for efficient generation of large masses of iPSCs[34] Using these systems in closed circuits could further simplify their use under Clinical Good Manufacturing Practice (cGMP) conditions. We previously implemented PBS mini–Vertical Wheel® Bioreactors for ~100-fold iPSC expansion[38] and achieved high efficiency in pancreatic progenitor cell differentiation (>90% PDX1 + NKX6.1 +)[24]. While these studies focused on iPSC expansion and progenitor production, they did not address the differentiation process.

Herein, we report on the utilization of PBS mini-Vertical-Wheel® (VW®) bioreactors in a single-vessel-single batch process generation of human iPSC-derived islet differentiation. By applying this throughout the process, we eliminated the need for any 2D planar culture and cell disaggregation-aggregation steps. Adapting the protocol from Sui et al.[13,39] we applied aphidicolin (APH), a potent cell growth inhibitor to further mitigate risk of off-target cells and cellular heterogeneity. Human iPSCs were seeded as individual cells and cultured as 3D clusters within VW® suspension bioreactors before differentiation, progressing through stages of definitive endoderm, pancreatic progenitors, and ultimately, functional islet-like cell differentiation 27 days. To assess the efficacy of our SC-islet cell manufacturing process, we compared our products to adult human cadaveric isolated islets in terms of cell composition, molecular, transcriptional, and functional maturation. We characterized the reproducibility of our SC-islet generation process using multiple iPSC lines and repeated differentiation batches across small (0.1 L) to scale-up (0.5 L) bioreactor vessels.

Our findings offer insight into the dynamics of scaling up process development, cell quality, cell composition, single-cell transcriptomics, and unwanted cellular heterogeneity. This linear progression of differentiation efficiency allows for the characterization of population heterogeneity and functional efficacy both during in vitro SC-islet differentiation and subsequent in vivo engraftment in immunodeficient mice. We demonstrate consistent generation of SC-islets from expansion through all stages of differentiation from 0.1 to 0.5 L reactors. We further investigate the impact of aphidicolin in reducing cell proliferation, enhancing endocrine cell maturation, and eliminating the need for physical disaggregation-aggregation of final cell products to minimize off-target cell populations.

Results

Vertical-Wheel® suspension bioreactors promote islet cell differentiation and offers scale up capacity of human SC-islets

Previously, we demonstrated successful derivation of genomically stable iPSC lines derived from peripheral mononuclear cells (PBMCs) from human subjects with and without diabetes[38]. For the current study, we used these patient-derived iPSC lines after quality control pluripotency characterization, viral clearance, normal karyotyping, mycoplasma absence, and pluripotent stem cell transcriptomics[38]. iPSC lines were expanded within VW® bioreactors to generate uniform 3D clusters. During expansion, a single iPSC expansion cycle in a 0.5 L VW® bioreactor vessel generated 997.1 (IQR: 850–1050) million human iPSCs with uniform 3D clusters of average 250 µm size (IQR: 125–324 µm), as previously reported by Cuesta-Gomez et al. from our group[38]. Following expansion, we designed an improved 27-day seed train for complete suspension differentiation of iPSCs into pancreatic islet cells adopting previously published differentiation protocol with modifications (Fig. 1a)[13,39]. The improved full-suspension, six-stages (S1 through S6) differentiation process efficiently produced islet-like clusters from each of the three tested iPSC lines in small (0.1 L) to scale-up (0.5 L) vessel (Supplementary Fig. 1a).

Directed differentiation of 3D iPSC aggregates in complete suspension condition across six-stages of pancreatic differentiation produced homogeneous 3D SC-islet aggregates at stage (S)-6. After 1 week of culture in stage-6, SC-islet clusters (henceforth termed "S6w1") resembled like human

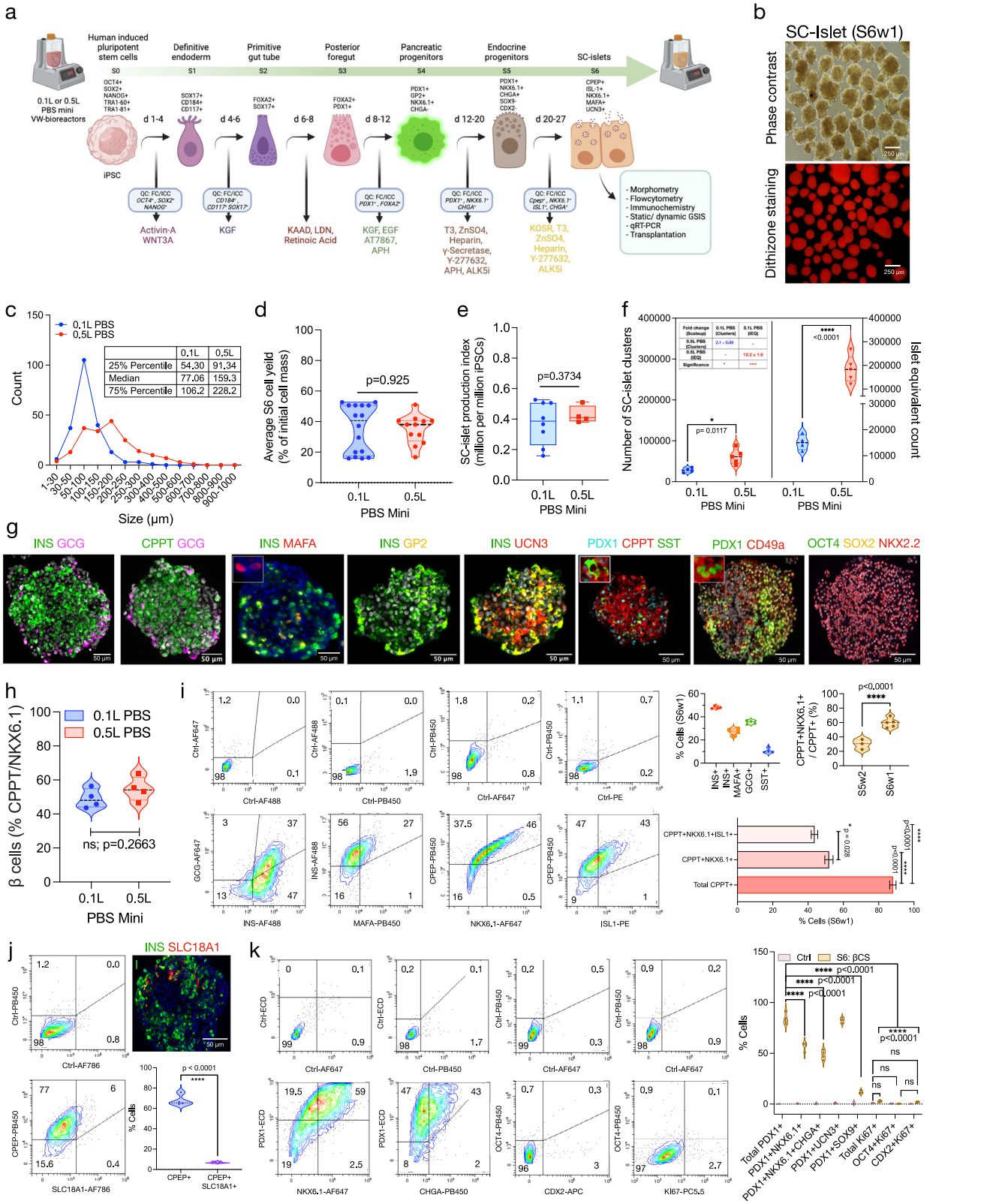

islets, morphologically. In both scales, S6w1 clusters stained positive for the zinc-binding dye dithizone (red), confirming the presence of insulin-stored β-like cells (Fig. 1b). This protocol generated SC-islet clusters of median size 77.06 µm (IQR: 54.30-106.2 µm; $n = 210$) in a 0.1 L vessel and 159.3 µm (IQR: 91.34–228.2 µm; $n = 193$) in a 0.5 L bioreactor vessel (Fig. 1c). The islet size distribution curve indicates that maximum clusters are generated within optimal islet diameter (<150 µm), and the frequency of large clusters is minimal across both scaling formats, enabling SC-islet scale-up without variability. We found linear scaleup efficiency for fully differentiated S6 cells after 27 days of differentiation without detriment to the final cell yield ($p = 0.925$; $n = 13$–16 batches) comparing 0.1 L and 0.5 L vessels. A single 0.1 L vessel yielded a median

Fig. 1 | Scale-up potential of Vertical Wheel® bioreactors in the generation of human pancreatic islets from induced pluripotent stem cells. a Overview seed-train of 27-day six-stage suspension culture differentiation protocol using VW® bioreactors with quality control release parameters and stage-specific growth factors added to each stage. Created in BioRender. Dadheech, N. (2025) https://BioRender.com/u86j668. Stages 1–7 termed as S1: definitive endoderm, S2: primitive gut tube, S3: posterior foregut, S4: pancreatic progenitors, S5: endocrine progenitors, S6: SC-islets. **b** Phase contrast and brightfield images of SC-islets for morphology and dithizone staining (red) to confirm islet differentiation. Scale bars, 250 µm. **c** Quantification, and size distribution of SC-islet clusters generated from 0.1 L and 0.5 L bioreactor vessels. Unpaired parametric *t*-test was performed with 95% confidence interval. All data are presented as median (IQR-27–75%), $n = 190–210$. **d** Violin plot representing average generation S6 cell as percentage of initial cell mass between 0.1 L and scale-up 0.5 L volumes. One-way analysis of variance (ANOVA), multiple comparison using Turkey correction with 95% confidence interval. All data are presented as mean ± sem, $n = 11–13$ pooled differentiation batches generated using three iPSC lines from healthy, total pancreatectomy, and type-1 diabetes donors (3–4 batches per line), *p* value statistically non-significant. **e** Box plot to show SC-islet production index-million S6 cells differentiation per million iPSCs between 0.1 L and scale-up 0.5 L volumes. One-way analysis of variance (ANOVA), multiple comparison using Turkey correction with 95% confidence interval. All data are presented as mean ± sem, $n = 4–8$ pooled differentiation batches generated using healthy, total pancreatectomy, and type-1 diabetes donor iPSC lines, *p* value statistically non-significant. **f** Graphical representation to show violin plot quantification (left axis) for total number of SC-islet cluster generation and (right axis) corresponding islet equivalent count measurements between 0.1 L and 0.5 L vessels. Two-way ANOVA with multiple comparison statistical method was used adopting Šidák correction with 95% confidence interval. All data are presented as mean ± sem, $n = 4–5$ pooled differentiation batches generated using healthy, total pancreatectomy, and type-1 diabetes donor iPSC lines. $^{*}p < 0.05$ and $^{****}p < 0.0001$. **g** Immunohistochemistry of day 27 harvested SC-islets from a health iPSC line probed with endocrine cell and pluripotency markers. Scale bars, 50 µm. **h** Violin plot representing quantification to measure the efficient for absolute SC-β cell generation within 0.1 L and scale-up 0.5 L bioreactor vessel. **i** Representative flow cytometry plots (left) marking islet cells in S6w1 SC-islets for markers- Insulin, Glucagon, Somatostatin, MafA, C-peptide, NKX6.1, and ISL1. Quantification graphs (right) show percentage cell count for Insulin, Glucagon, MAFA, Somatostatin, C-peptide, and NKX6.1 in S6w1 SC-islets. One-way analysis of variance (ANOVA), multiple comparison using Turkey correction with 95% confidence interval. All data are presented as mean ± sem, $n = 4-5$ pooled differentiation batches generated using healthy, total pancreatectomy, and type-1 diabetes donor iPSC lines. $^{*}p < 0.05$ *and* $^{****}p < 0.0001$. **j** Representative flow cytometry plots and quantification for enterochromaffin cell generation within the SC-β cells in S6w1 clusters. Multiple ttest statistical method is used to compare two variables with 95% confidence interval. All data are presented as mean ± sem, $n = 4$ pooled differentiation batches generated using healthy, total pancreatectomy, and type-1 diabetes donor iPSC lines. $^{****}p < 0.0001$. Immunohistology image show staining for SC-EC marker-SLC18A1 co-labeling with insulin. Scale bars, 50 µm. **k** Representative flow cytometry plots (left) to show absolute cell composition for off-target population in S6w1 SC-islets. Violin plot (right) show quantification of percentage off-target cells generated in comparison to isotype control. Two-way ANOVA with multiple comparison statistical method is used with Šidák correction and 95% confidence interval. All data are presented as mean ± sem, $n = 3–4$ pooled differentiation batches generated using healthy, total pancreatectomy, and type-1 diabetes donor iPSC lines. $^{****}p < 0.0001$.

40.6% S6 cell mass IQR: 15.7–52.6% (79.3 ± 4.8 million cells) and was transferable to 0.5 L scaleup without change- 38.1% S6 cell mass: IQR: 16.67–51% (213 ± 9.6 million cells) (Fig. 1d). We observed a consistent SC-islet production index (calculated as "million S6 cells differentiated per million iPSCs"), moving from 0.1 L to scale-up 0.5 L without significant difference ($p = 0.3734$; $n = 4–8$ batches). An islet index of 0.39 million S6 cells per million iPSCs (IQR: 0.23–0.50) was observed in 0.1 L vessels compared to 0.41 million cells per million iPSCs (IQR: 0.39-0.49) (Fig.1e). We found S6 cell yield, and islet cell production index was both consistent and reliable without variation and heterogeneity.

We then compared the total SC-islet cluster numbers and IEQ generated across two vessel sizes and observed significant increase in both cluster numbers and the IEQ census. A 0.1 L vessel produced a median of 28,050 SC-islet clusters (IQR: 23,087–33,687), while a 0.5 L vessel produced a median of 61,083 SC-islet clusters (IQR: 44,827–78,625), demonstrating a 2.1 ± 0.09-fold increase in SC-islet cluster generation after a 5× increase in vessel size ($p = 0.0117$, $n = 4-5$). Over the past 25 years, IEQ measurement of islet volume has been used as a gold standard for islet mass dosing when applied to clinical islet transplantation. Islets may be considered as 3D organoid structures, and the overall cell mass within the islet cluster is more representable with IEQ volume measurement rather than number[40]. We extrapolated the total IEQ generation between the two vessel sizes and the efficiency of scale up was 12.2 ± 1.6-folds ($p < 0.0001$; $n = 4–5$) within 5 times volume testing compared to 2.1 ± 0.09-fold increase in cluster number, suggesting a relevant increase in overall cell mass production. A total of 183,002 IEQ (255,558–134,300) were produced from a single 0.5 L vessel and 15,005 IEQ (IQR: 12,350–18,020) in 0.1 L vessel (Fig. 1f).

After directed differentiation of iPSCs into islet cells for 27 days in full suspension culture, these SC-islets resembled primary islet clusters and showed the presence of all human islet hormones. S6w1 cells were stained for islet makers including: Green: Insulin (INS), C-peptide (CPPT), Somatostatin (SST) Pancreatic duodenal homeobox-1 (PDX1), Red: C-peptide (CPPT), Urocortin-3 (UCN3), MAF bZIP transcription factor A (MAFA), CD49a, and Homeobox protein Nkx-2.2-like (NKX2.2); Yellow: Glycoprotein-2 (GP2), Cyan: PDX1; and Pink: Glucagon (GCG). All pluripotency associated genes including Green: Octamer-binding transcription factor 4 (OCT4) and Yellow: SRY-related HMG-box (SOX2) were not seen in SC-islets (Fig. 1g). S6w1 clusters represent mono-hormonal cell populations for β-like (INS+GCG-), α-like (GCG+INS-), and few poly-hormonal cells. Additionally, co-staining for INS with CPPT suggest that new β-like cells have fully developed. MAFA, a mature β cell-specific transcription factor, was found to be co-stained with INS in β-like cells in the clusters. We observed GP2 and UCN3 staining in islets alongside INS, indicating maturation of β-like cells. S6w1 islets showed PDX1 (cyan) transcription factor staining only in CPPT+ (red) cells, whereas SST+ cells were identified as distinct population (enlarged inset). Co-labeling for PDX1 (green) and CD49a (red), a surrogate marker of secretory mature β-like cells confirmed the presence of an endocrine-rich population, as previously reported by Veres et al.[14]. Finally, we observed homogenous staining for transcription factor NKX2.2 in S6w1 clusters but there was no evidence for off-target undifferentiated cell markers- OCT4 and SOX2, suggesting high purity of endocrine cell populations without residual contamination (Fig. 1g).

Bioreactor developed SC-islets attain endocrine cell composition

To assess the utility of VW® suspension bioreactors for SC-islet differentiation, we characterized cell composition of 3D clusters from the beginning of differentiation at the definitive endoderm stage (S1) through to the end of islet cell maturation stage (S6) using both immunochemistry and flow cytometry. Cells differentiated during definitive endoderm stage within VW® bioreactors showed efficient definitive transition into endodermal cells (S1), as illustrated by nuclear SOX17 (red) and cytoplasmic CD117 (green) co-labeled immunostaining (Supplementary Fig. 1b). Harvested single S1 cells revealed the presence of $CD184^{+}CD117^{+}$ (96.93 ± 1.6%; $p < 0.000001$; $n = 7$), $SOX17^{+}CD117^{+}$ (92.18 ± 1.5%; $p = 0.000001$; $n = 7$), and $SOX17^{+}FOXA2^{+}$ (93.98 ± 1%; $p = 0.000001$; $n = 5$) immunopositivity (Supplementary Fig. 1b). Endodermal S1 cells differentiated into $CD117^{+}FOXA2^{+}$ (87.09 ± 1.3%; $p < 0.000001$; $n = 8$) cells in S2 (Supplementary Fig. 1c) and transitioned into the early pancreatic progenitor stage at S3.

At S3, differentiating clusters represented a total of 95.4 ± 0.8% PDX1 cells ($p < 0.0001$; $n = 5$). Of these, 41.3 ± 4.4% of cells retained PDX1 + FOXA2+ expression ($p < 0.0001$.; $n = 5$) prior to pancreatic progenitor differentiation (S4) (Supplementary Fig. 1d). At S4, over

96.8 ± 0.99% of these cells were PDX1$^+$ progenitors. Of these, 90.4 ± 0.99% cells ($p = 0.0001$; $n = 8$) co-expressed PDX1$^+$NKX6.1$^+$, and a significantly lower population of 49.9 ± 8.0% cells ($p < 0.0001$; $n = 7$) showed CHGA$^+$NKX6.1$^+$ expression. S4 cells also retained pancreatic progenitor marker expression with 86.4 ± 5.1% GP2+ ($p < 0.0001$; $n = 7$) (Supplementary Fig. 1e), as reported previously by Nostro et al.[23,41]. After transitioned to S5, developing clusters (now referred to as S5w2) had a high proportion of CHGA (green) and NKX6.1 (red) stained cells immunohistochemically. Absolute quantification of S5 cells revealed 64.5 ± 5.2% CHGA$^+$NKX6.1$^+$ ($p < 0.0001$; $n = 3$), a significantly higher population of endocrine progenitor cells than in earlier stages, of which 28 ± 3.9% cells showed the presence of CPPT$^+$NKX6.1$^+$ cells (Supplementary Fig. 1f).

At terminal differentiation (27 days), S6w1 clusters harvested from 0.1 L and scale-up 0.5 L vessels represented a comparable SC-β population (CPPT$^+$NKX6.1$^+$) without significant difference (0.1 L: 48.07% [IQR-44.13–54.90%]; 0.5 L: 54.08% [IQR-48.16–61.50%], $p = 0.2663$, $n = 4$) (Fig. 1h). Collectively, S6w1 cells showed a total of 88.1 ± 1.8% CPPT$^+$ cells of which 51.8 ± 2.3% co-expressed CPPT$^+$/NKX6.1$^+$ markers and 43.6 ± 1.8% co-expressed CPPT$^+$/ISL1$^+$ markers ($p < 0.0001$, $n = 6$); of these 49.5–50% cells are positive for endocrine CD49a marker (Supplementary Fig. 1g) confirming β-like phenotype and composition similar to adult human donor islets (Fig. 1i; Supplementary Fig. 10a–c). We defined S5w2 for immature and S6w1 for mature islet cells in S6. Following maturation from S5w2 to S6w1, the proportion of cells expressing CPPT$^+$NKX6.1$^+$ increased from 29.9 ± 4.0% to 59.5 ± 2.9% cells ($p < 0.0001$, $n = 3$–5) (Fig.1i). Within these mature S6w1 clusters, we observed 48.06 ± 0.6% INS, 35.53 ± 0.8% GCG, and 10.39 ± 1% SST single hormonal cells, while there were 27.07 ± 1.5% INS cells that co-stained with MAFA (Fig.1i).

Presence of serotonin secreting EC cells is often associated with poor differentiation into endocrine cells, several investigations has shown that least frequency of SC-EC cell-SLC18A1$^+$ generation is a direct reflection of mature SC- β population generation. Reassuringly, in our total CPPT$^+$ population, only 6.8 ± 0.4% of cells co-stained for the enterochromaffin lineage marker, SLC18A1 and 6.6% LMX1A (Supplementary Fig. 11a). The frequency of enterochromaffin cells was further validated immunohistochemically by labeling the S6w1 cluster with INS (green) and SLC18A1 (red) (Fig. 1j). In addition, a total of 83.9 ± 2.8% of our cells were PDX1$^+$, of which 56.9 ± 2.1% ($p < 0.0001$; $n = 4$) were PDX1$^+$NKX6.1$^+$ and 48.5 ± 2.3% ($p < 0.0001$; $n = 4$) were PDX1$^+$CHGA$^+$NKX6.1$^+$ (Fig. 1k). Examining the PDX1$^+$ cells in our S6w1 clusters revealed that 82.6 ± 1.6% were PDX1$^+$UCN3$^+$ expressing with only 11.9 ± 0.9% cells ($p < 0.0001$, $n = 4$) cells expressing the ductal phenotype, PDX1$^+$SOX9$^+$. Reassuringly, our S6 population displayed minimal frequency of proliferation and off-target cell markers with 2.23 ± 0.5% of Ki67$^+$, 0.33 ± 0.1% Oct4$^+$/Ki67$^+$ cells, and 1.9 ± 0.3% as CDX2$^+$/Ki67$^+$ cells (Fig. 1k). Overall, our results from stage-specific cell composition analysis using flow cytometry confirmed efficient endocrine cell differentiation without off-target cell contamination and minimal proliferation.

Suspension SC-islets show in vitro functional potential and glucose-responsive insulin release

To assess the functional maturation of our SC-islets differentiated in VW® bioreactors, we performed dynamic continuous and static glucose stimulated insulin secretion (GSIS) assays and compared immature S5w2 clusters and mature S6w1 islets against adult islets as control (Fig. 2a). In dynamic assay, adult islets (brown) exhibited finely regulated insulin secretion response after changes in glucose concentration from 3 mM to 17 mM and final depolarization with 30 mM KCl. In comparison, matured S6w1 SC-islets (green) showed modest fold change in secreted insulin with glucose stimulation, although at a lower capacity than adult islets. When incubated in high glucose for 13–32 min, both mature S6w1 (peak at 20 min, S6w1: 6.6 ± 0.2 fc over G3; $p = 0.0267$, $n = 5$–6) and adult islets displayed significant increase in insulin secretion compared to immature S5w2 clusters. However, in KCl depolarization for 33-44 min, S6w1 clusters were comparable to adult islets and S5w2 cells (Fig. 2a). Convincingly, immature S5w2 clusters (pink) failed to respond at varying low to high glucose concentrations and only secreted after KCl depolarization (Fig. 2a). Significant change in area under the curve for perifusion tracing in S6w1group displayed the functional potential and maturation of SC β cells, compared to immature S5w2 cells ($p = 0.0073$, $n = 5$–6) (Fig. 2b).

Additionally, static incubation of S6w1 islets with low, high glucose, and KCl displayed a significant increase in insulin secretion. A thousand S6w1 cells produced a total of 4.9 ± 1.2 μIU insulin/ml in high glucose compared to 0.9 ± 0.2 μIU insulin/ml in low glucose ($p = 0.0889$; $n = 4$) which was comparable to an adult donor islet secretion capacity (Fig. 2c), indicating functional responsiveness of SC-β cells. Further, we then measured difference in the secretion capacity of S6w1 cells generated within two vessel sizes. We observed no statistical difference in fold change over low glucose between the 0.1 L and 0.5 L generated cells (Fig. 2d). Both 0.1 L and 0.5 L batches demonstrated median fold 3.6 [IQR: 2.2–5.1] and 7.01[IQR: 3.2–11.9] changes respectively after low to high glucose transition. Notably, our data suggested similar functional capacity of SC-β cell generation during scale-up.

This functional in-vitro maturity of S6w1 SC-islets can be explained by transcriptional changes that happened during the transition from S5w2 to S6w1. Transcription factors involved in the insulin signaling pathway (*CHGB, PCSK1N, KCNK3*) were promoted in S6w1 clusters compared to S5w2 immature cells (Fig. 2e). Glycolysis and TCA pathway-related genes (*G6PC2, GCK)* were also upregulated in S6w1 mature β cells (Fig. 2e). Heatmap cluster matrix analysis of maturation-associated genes shows upregulated expression of functional transcripts in two independent batches of S6w1 SC-islets (red) than S5w2 islets (cyan) (Fig. 2f). Violin plots for glucose control regulating genes (*PSCK1/2, GCK, G6PC2*) along with exocytosis controlling genes (*KCNK1/3, GLP1R, CHGB*) showed upregulated in S6w1 cells compared to immature S5w2 cells (Fig. 2f). Overall, when compared with two different batches of adult islets and their mature β cell signatures- combined matrix maturation associated genes, S6w1 SC-islets have higher degree of similarly in expression levels compared to S5w2, as illustrated in Fig. 2f. Again, expression plots for islet maturity markers showed marked upregulation for *INS, IAPP, SLC30A8*, and *MAFA* in S6w1 cells compared to S5w2 cells (Fig. 2g), suggesting that suspension differentiation improves SC-islet maturation and the activation of exocytosis machinery.

Suspension SC-islets reverse diabetes after in vivo maturation

To investigate the in-vivo function and maturation of suspension-generated S6w1 cells, we transplanted S6w1 SC-islets under the renal sub capsule in streptozotocin (STZ)-induced diabetic immunodeficient SCID beige mice (Fig. 3a). We monitored serum glucose levels of the transplanted mice for over 16 weeks to assess functional efficacy and long-term engraftment. Non-transplanted STZ-induced diabetic control mice (red) exhibited elevated glucose levels >20 mM over 90 days (Fig. 3b). Mice transplanted with S6w1 clusters (green) displayed a rapid decline in blood glucose within 30 days post-transplant which persisted until 105 days when the grafts were harvested for histological analysis (Fig. 3b). S6w1 transplanted mice showed significantly lower area under the curve compared to non-transplanted diabetic mice ($p < 0.0001$; $n = 4$–15). A Kaplan-Meier curve for diabetes reversal highlighted successful engraftment and functional maturation of transplanted SC-islet grafts. More than 50% of transplanted mice ($n = 15$) achieved euglycemia within 30 days post transplantation ($p = 0.0344$). At 60 days, all transplanted mice ($n = 15$) showed reversal of STZ-induced diabetes and improved glycemic control from graft function (Fig. 3c).

Intraperitoneal glucose tolerance tests (IPGTT) were performed in these mice which revealed significantly improved glucose tolerance at 16 weeks post-transplant in S6w1 mice compared to diabetic controls ($p = 0.0026$ at 30 min, $p = 0.0003$ at 60 min, and $p = 0.0031$ at 90 min of glucose infusion, $n = 4$–10) (Fig. 3d). Human C-peptide secretion in diabetes reversed animals after glucose infusion demonstrated mean fasted c-peptide levels of 135.9 ± 51.2 pmol/L and 721.8 ± 259.1 pmol/L at 60 min glucose-stimulation at 16 weeks post-transplantation (Fig. 3e). We also

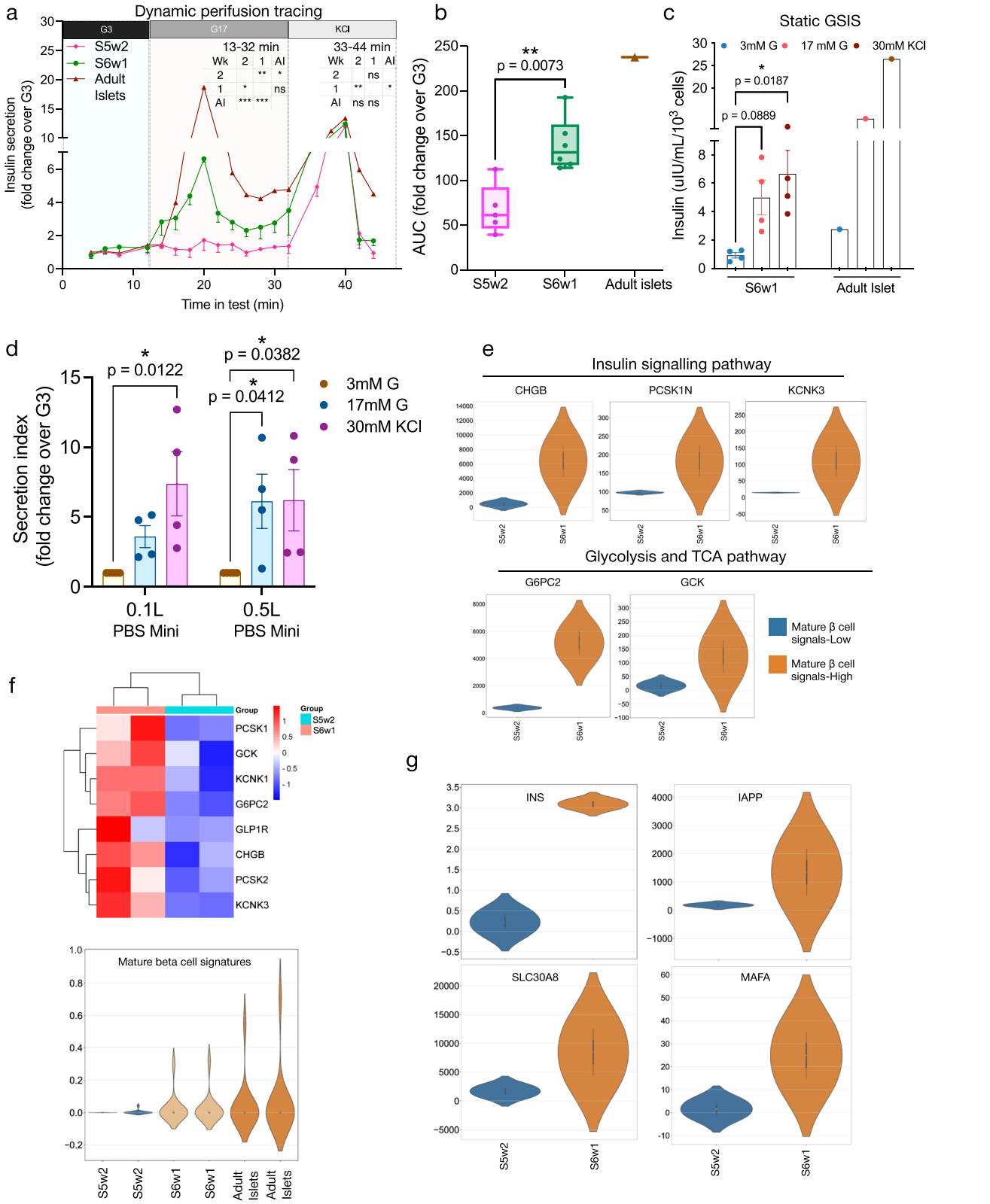

measure stimulated human insulin secretion in transplanted mice at 16 weeks ranging from 0.28 ± 0.06 to 0.69 ± 0.05 ng/ml within 60 min after glucose infusion (Supplementary Fig. 11b). In time course evaluation, we observed gradual and progressive improvement in glycemia control and C-peptide secretion between 8–16 weeks duration, demonstrating in vivo competence of engrafted cells. At 8 weeks post-transplant, stimulated C-peptide secretion (fold change to fasting) was recorded at 0.8 ± 0.08, which increased to 1.52 ± 0.2 at 12 weeks ($p = 0.0066$, $n = 4$) and 3.10 ± 0.49 ($p = 0.0001$, $n = 4$) at 16 weeks (Fig. 3f). Collectively, glucose responsive IPGTT and human c-peptide release after stimulation confirmed that the graft is active, survived and attained the maturity level required for glucose responsiveness and correct diabetes.

Fig. 2 | In vitro functional characterization of SC-islets. a Insulin secretion response to dynamic perifusion with 2.8 mM (G3), 16.7 mM (G17) glucose, and 30 mM KCl. Secretion tracing was normalized to total DNA content *(n = 3)* from S6w1 (50 clusters) islets in 2 technical replicates from three independent differentiation batches—one from each healthy, total pancreatectomy, and type-1 diabetes donor iPSC lines tested. **b** Quantification of area under the curve from perfusion tracings between S5w2, S6w1, and donor islets. **c** Static insulin secretion response to varying glucose concentrations from G3 to G17 and KCl from S6w1 (30 clusters) islets in comparison to adult donor islets. Insulin levels are normalized per 1000 cells, $n = 4$ differentiation batches using a healthy iPSC line. Average secretion of technical replicates, $n = 2$, is plotted from a single representative donor islet. Two-way ANOVA with multiple comparison using Šidák correction with 95% confidence interval. All data are presented as mean ± sem, $n = 4$. $^{*}p < 0.05$, $^{**}p < 0.001$, and $^{****}p < 0.00001$. **d** Graphical quantification of secretion index (fold over G3) in S6w1 (30 clusters) islets upon G17 and KCl stimulation moving from 0.1 L to scale-up 0.5 L bioreactor vessel. Two-way ANOVA with multiple comparison statistical method is used with Šidák correction and 95% confidence interval. All data are presented as mean ± sem, $n = 4$ differentiation batches from a healthy iPSC line. $^{*}p < 0.05$. **e** Violin plots representing average expression of genes responsible for insulin signaling and glycolysis-TCA cycle pathway. **f** Heatmap projection (top) of average gene expression profile in S6w1 islets generated from healthy donor iPSC line ($n = 1$) against immature S5w2 clusters for genes associated with glucose metabolism and secretory function. Violin plots (bottom) representing matrix of mature beta cell gene expression measured in S5w2 clusters and S6w1 islets compared to adult islets **g** Violin plots representing level of expression of maturation genes in comparison between immature S5w2 clusters and mature S6w1 islets from time of origin. Heat map and violin plots are generated using SR Plots bioinformatics online tool https://www.bioinformatics.com.cn/en.

At 3 months post-transplantation, grafts were harvested, and tissues were assessed for graft histology and immunophenotyping. S6w1 grafts demonstrated the presence of mature all islet cell types within the engrafted tissues. These include the presence of- β-like (INS), α-like (GCG), δ-like (SST), and Ghrelin-like (GHRL) cells (Fig. 3g). We found that majority of endocrine INS and GCG positive cells engrafted separately and became mono hormonal within the endocrine tissue niche, indicating that endocrine maturity and engraftment has occurred. Only a small fraction of graft tissue has acquired a combined staining for INS and GCG, suggesting the presence of immature polyhormonal cells. Furthermore, we observed the presence of endocrine maturation markers- GP2, UCN3, and MAFA along with INS to confirm grafted-β cells in-vivo maturation.

We then documented the evidence for vascularization by marking vascular cells for CD31 in INS rich areas, and expectedly confirmed S6w1 graft stained positive for vascular CD31 cells. Additionally, only marginal areas of graft tissues were co-stained Ki67, a marker of proliferation with INS, suggesting the presence of immature proliferating β-like cells at a very low frequency (Fig. 3g). Histological assessment of harvested grafts after 3-months post-transplant demonstrated the development of endocrine tissue morphology in the renal subcapsular space (Fig. 3h). Although grafts were highly enriched for endocrine tissue, particularly few areas within histology also stained for ductal maker- cytokeratin 19 (CK19). Immunohistochemical staining demonstrated survival and engraftment of residual pancreatic progenitor cells that gradually developed into ductal or microcystic structures, possibly from contaminating non-endocrine cells (Fig. 3h). Histologically, we did not observe any evidence for pancreatic intraepithelial neoplasia or ductal hyperplasia in S6w1 grafts.

We then investigated the molecular genomic architecture and cell composition of harvested graft tissues using single cell dispersion of graft-harvested tissues from 3–4 animals at 8- and 16-weeks post-transplantation. Graft isolated single cells were characterized for their gene expression of key pancreatic developmental, maturation, and functional genes using TaqMan gene array cards (Fig. 3i) and flow cytometry (Fig. 3j). Gene array quantification for 48 islet maturation genes was generated to assess the in-vivo maturation of graft-matured tissues in reference to SC-islets prior to transplantation. Gene array configuration and comparative statistics for each gene are described in Supplementary Material Table S7. We explanted grafts from 3 mice at 2-months (green) and 4 mice at 4-months (pink) post-transplantation and normalized the expression to S6w1 pre-transplant cells (blue, baseline control) (Fig. 3i). Our data suggested downregulation for pluripotency associated genes such as *POU5F1, SCL24A*, and *SLC16A1* in purified S6w1 cells with marked upregulated for islet markers (*INS, ARX, CHGA, PAX4, ISL1*, and *NEUROD1)*, functional (*MAFA, ABCC8, PCSK1, KCNK3, SLC30A8, GCK, G6PC2, GLP1R*) and maturation (*IAPP, UCN3, NKX6.1, ITGA1*) genes (Fig. 3i).

At 2-month post-transplantation transcriptional landscape of harvested graft cells from three mice showed varying levels of gene transcripts; but the majority of functional genes were not significantly upregulated compared to pre-transplant S6 cells. Likewise, at 4-months post-transplantation, we observed a consistent upregulation of endocrine rich transcripts for mature islet cells, including- *IAPP, MAFA, UCN3, GP2, PAX6, CPE, TSPAN1, NKX6.1, CHGB, ISL1, ITGA1, CXCR4, UCN3* and *SOX17* compared to pre-transplant cells. These observations conclude that SC-islets continue to mature in-vivo and that this process takes several months to establish the endocrine islet maturation identity (Fig. 3i). Notably, 4 months harvested graft cells also confirmed significant upregulation for functional exocytotic genes (*ABCC8, PCSK1, KCNK3, SLC30A8, GCK, G6PC2, GLP1R, MAFA/B, PCSK2)* and improved β cell functionality (Fig. 3i).

Flow cytometry quantification of single dispersed cells from 4-month graft harvested tissue (n = 3–5 mice) confirmed endocrine cell composition in graft tissues. Each harvested graft tissue consisted of ~77% endocrine cell types, while 23% were other cells (non-endocrine phenotype). Of these 77% endocrine cells, 26% were identified as SC-derived mature β cells, 6% as proliferating β cells, 24% as pancreatic progenitor cells, and the remaining 44% cells were counted as endocrine progenitor cells (Fig. 3j). When compared for parts of whole graft analysis, the major cell types covered the tissue composition were- 9.3% INS, 1.09% GCG, 1.06% SST, 16.61% CHGA, 12.01% PDX1, 6.61% NKX6.1, 5.18% PDX1-NKX6.1, and 12% PDX1-CXCR4 cells. Only a small fraction of endocrine cells (1.46%) was identified as SC-EC cells- SLC18A1 and no evidence of off-target PSCs was captured within the graft tissue composition.

Suspension SC-islets transcriptionally mature in vitro

To investigate the transcriptional maturation SC-islets and changes over time- S1-S6, in vitro, we performed stage specific transcriptional tracing of key islet developmental genes using Taqman Low Density Genes Array (TLDA) cards. We compared the transcriptomics of forty-eight canonical pancreatic differentiation pathway genes between datasets of S1 to S6 cells *versus* adult islets and undifferentiated controls. Gene encoded in TLDA card array configuration can be found in Supplementary Material Table S7. Cluster analysis with heatmap for forty-eight genes of three independent SC-islet (S6w1) batches was comparable to adult islet from three donors (Supplementary Fig. 2a). Manhattan nearest neighboring clustering in replicate batches of SC-islets, donor islets, and undifferentiated iPSCs clustered SC-islets and adult islets as nearest neighbor based on similar gene transcripts. Likewise, relative gene expression for several endocrine genes were gradually upregulated moving from S1 to S6 confirming endocrine transcriptional programming, while progenitor and off-target genes were downregulated during terminal stages of differentiation (Supplementary Fig. 2b). We specifically compared for β cell maturation-related genes including *MAFB, PCSK1/2, G6PC2, ITGA1, SLC30A8 (ZnT8), CPE*, and *TSPAN1*. At day 27, we observed upregulation for crucial β cell identity and insulin secretion associated genes similar to donor islets. These includes *INS, ISL1, PDX1, UCN3, NKX6.1, GP2, CHGB, NGN3, NEUROD1*, and *PAX4*. S6 cells at day 27 were also enriched for α cells associated genes- *ARX, CHGB, ISL1, and MAFB*. Importantly, off-target pluripotency associated gene-*POU5F1* showed significant downregulation and turned off after 27 days of differentiation (Supplementary Fig. 2b).

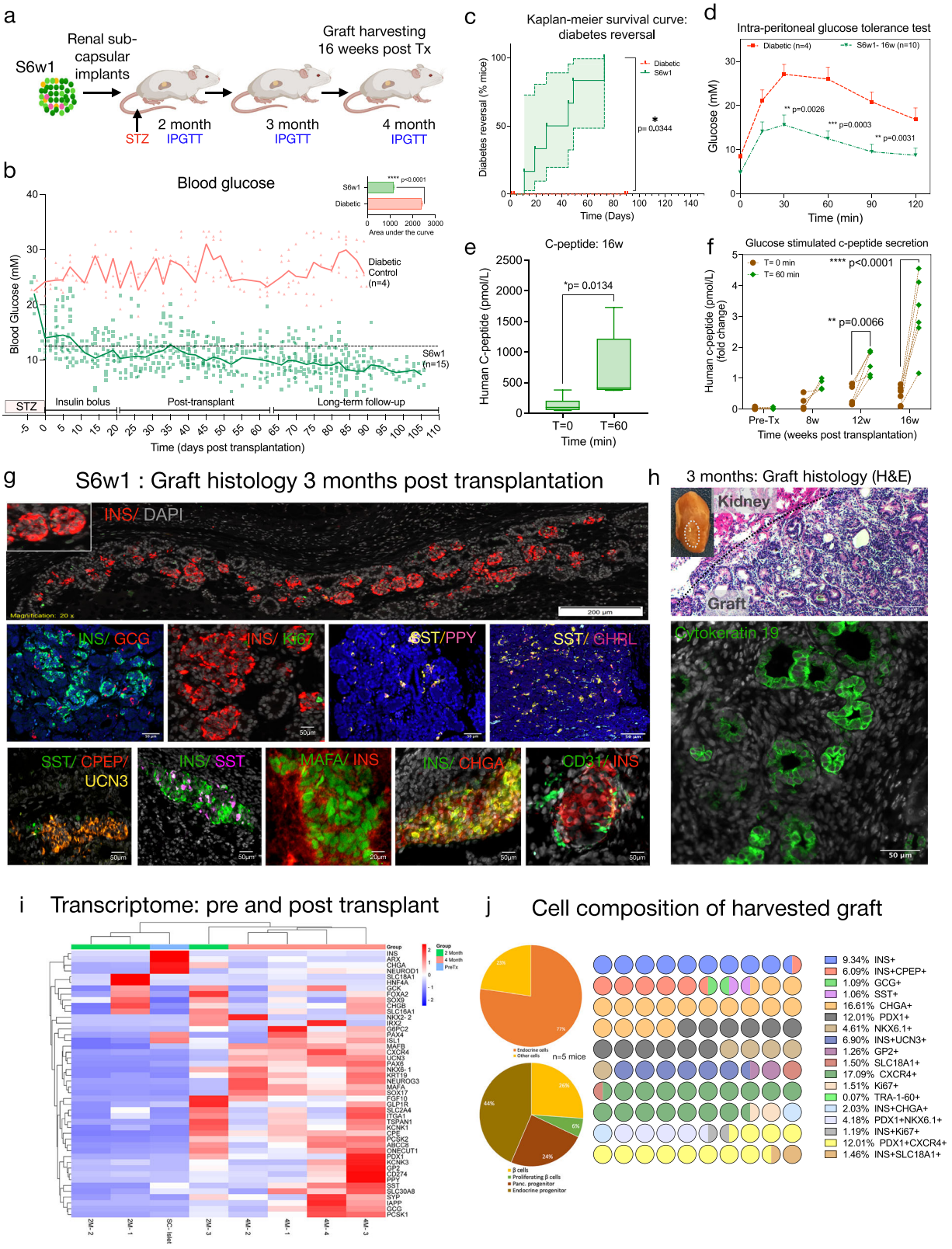

Next, we conducted bubble plot correlation analysis to compare S5w0 and S6w1 islets to human donor islets. These revealed intense upregulation for these genes moving from day 0, 4, 12, and peaked at day 27. (Supplementary fig. 2c). We compared average gene expression for β cell maturation markers- *INS, GCG, UCN3, NEUROD1, MAFA*, and *CHGA* at day 0, 4, 12, and 27. We observed rapid increase in transcript levels for SC-β cell markers from day 12 and peaked at d27, whereas progenitor marker expression for *NEUROG3, PDX1, PAX4*, and *GP2* were maintained throughout the differentiation. Interestingly, there was initial upregulation for *CD274 (PDL1)* and *TSPAN1* and was reduced in later stages to the equivalent levels of adult islets. Pluripotency associated gene- *POU5F1* transcript remained undetected at day 27, similar to adult islets (Supplementary Fig. 2c).

Fig. 3 | In vivo transplantation and maturation of SC-islets to reverse diabetes. **a** Schematic representation of transplantation approach and graft assessment timeline after 2, 3, and 4 months of transplantation in SCID-beige mice. Created in BioRender. Dadheech, N. (2025) https://BioRender.com/u86j668. **b** Random glucose monitoring after S6w1 islet transplantation to evaluate in vivo functional potential in correcting diabetes in immunodeficient SCID-beige mice. Diabetic control mice *(n = 4)* are marked in red, while transplanted reversed mice *(n* = 15; transplanted with three batches of SC-islets from healthy, total pancreatectomy, and type-1 diabetes donor iPSC lines*)* in green. Dotted black line represent a threshold to consider reversal and normoglycemia. Each mouse was implanted with a LinBit-insulin pellet (21 days) to control severe hyperglycemia after diabetes induction to allow for graft survival during early weeks of transplantation. Animals were monitored up to 105 days without glucose management. Mean area under the curve (top right) for each group represented glucose lowering effect from S6w1 islet transplantation for 4 months engraftment. Multiple *t* test statistical method is used to compare two variables with 95% confidence interval. All data are presented as mean ± sem, $n = 4$. $^{****}p < 0.0001$. **c** Kaplan-meier graph representing diabetes reversal in transplanted mice during 105 days of monitoring. *T* test statistical method with 95% confidence interval; $n = 4–15$ $^{*}p < 0.05$. **d** Quantification of in vivo functional efficacy after impaired glucose tolerance test at 4-months post transplantation in S6w1 engrafted mice. Two-way ANOVA and multiple comparison using Šidák correction with 95% confidence interval was performed. All data are presented as mean ± sem, $n = 4–10$ mice, $^{**}p < 0.01$ and $^{***}p < 0.001$. **e** In vivo glucose stimulated human c-peptide secretion from S6w1 transplanted mice at 4-months post transplantation. One-way ANOVA and multiple comparison using Turkey correction with 95% confidence interval. All data are presented as mean ± sem, $n = 6$, $^{*}p < 0.05$. **f** Time dependent human c-peptide secretion from S6w1 transplanted mice at 8-, 12-, and 16-weeks post transplantation before glucose infusion at $t = 0$ min and after $t = 60$ min of 3 g/Kgbwt glucose infusion. Two-way ANOVA with average mixed effect using Turkey correction with 95% confidence interval, at multiple time points comparison. All data are presented as mean ± sem, $n = 6$ mice, $^{**}p < 0.01$ *and* $^{****}p < 0.0001$. **g** Representative immunohistochemical images of graft harvested tissues from S6w1 transplanted mice after 16- weeks post transplantation stained for endocrine islet cells, proliferation, and vascularization markers. Scale bars, 50–200 µm. **h** Representative picture of whole harvested kidney with graft implanted with S6w1 islets in 16-week engrafted mice. H and E histological image displaying gross histology of graft embedded kidney and immunohistochemistry of endocrine graft region under renal subcapsular space demonstrating presence of ductal region, stained with Ck19 in a 16-weeks harvested tissue. Scale bars, 500–100 µm. **i** Heat map projection of islet differentiation and maturation gene clusters in 2- and 4-months engrafted mice, in comparison to S6w1 islets (average of 3 independent differentiation preps one from each healthy, total pancreatectomy, and type-1 diabetes donor) pre-transplantation. Color scale (top right) represents gene upregulation (red; >0) and downregulation (blue; <0), Graft assessment form $n = 3–4$ mice. SC-islet gene expression datasets are represented as an average of $n = 3$ independent batches from 3 donor iPSC lines. Heat map was generated using SR Plots bioinformatics online tool https://www.bioinformatics.com.cn/en. **j** Flow cytometry-based graft cell composition analysis as pi-chart quantification labeling as percentage of β cell, proliferating β cell, pancreatic progenitors, and endocrine progenitors. Graft cell composition is represented as heat map parts of whole representation in an entirety of harvested graft. $n = 4–7$ mice.

SC-islets exhibit single cell heterogeneity resembling to adult donor islets

We analyzed and compared the RNAseq datasets of S6w1 cells generated in VW® bioreactors with adult human pancreas (Azimuth-Satija Lab)[42–49] and isolated adult donor islets from three healthy donors (GEO accession# GSE217837)[50]. The alignment calculated the percentage annotated populations combining pancreas scRNAseq projections from pooled datasets gathered from different sequencing methodologies and human donors. Unimodal UMAP projection of S6w1 cells confirmed identity of thirteen pancreatic cell populations of which majority were annotated to β-like (36.80), α-like (22.60), δ-like (19.30), γ-like (1.60), and ductal (8.60) cells (Fig. 4a).

We performed clustering of S6w1 dataset and projected onto the human donor islet datasets obtained from GSE217837[50] and a total of 9 distinct clusters were identified on a UMAP projection (Fig. 4b**;** Supplementary fig. 2d). In combined UMAP projection, S6w1 cells were majorly clustered in 0, 1, 2, 4, and 5 clusters, whereas donor islets clustered in 0, 3, 4, 6, 7, 9, and 8. Feature plots projections for *INS* and *GCG* expression in S6w1 cells demonstrated marked insulin expression in a distinct cluster-2, along with scattered expression in clusters-1, 3 and 5, compared to cluster-3 in adult donor islets. Similarly, GCG expression was marked to clusters-0, 1, and 6, in S6w1 islets compared to cluster-0 in adult islets (Fig. 4c). Detailed expression profiling for S6w1 cells *versus* donor islets are summarized in Supplementary Fig. 3a. Differential gene expression (DGE) comparison between S6w1 islets *versus* adult donor islets revealed downregulation of 149 genes and upregulation of 303 genes on a volcano plot (Fig. 4d).

We outlined key β cell identity markers between S6w1 islets and adult donor islets using violin plots. Similar to adult donor islets, S6w1 islets displayed a bimodal distribution for *INS* transcript, albeit with less maturity. In particular, the lower distribution for high *INS* transcript expression suggests fetal-like S6w1 islets. Majority of *INS* expression was sparsely distributed suggesting modest S6w1 islet maturation. Convincingly, all other key markers for β cell identity (*PAX6, NKX2-2, MAFA*) and maturation (*GCK, ABCC8, PCSK1, G6PC2*) were expressed and resembled to donor transcript levels (Fig. 4e). A strong transcriptomic resemblance was observed between established canonical gene cell markers (*GCG, INS, SST* and *PPY*) along with known selective identity, maturation, secretion, metabolism and exocytosis markers for α, β, δ and γ cells (Supplementary Fig. 4a–d). We also compared and analyzed expression for MODY, proliferation and disallowed genes and found no significant differences for majority of genes, except for *LDHA, LDHB* and *HK1* disallowed genes (Supplementary Fig. 5a–c).

We further tested similarities of identified clusters in S6w1 scRNA-seq dataset for canonical genes as a hallmark of endocrine transcriptomics defining α, β, δ and γ cell populations, as described previously[51] (Fig. 4f). Dot plot analysis for endocrine cell population within each of the identified clusters presented a set of genes, including α (*GCG, SCG2, CRYBA2, TTR, ARX*), β (*INS, NKX2-2, DLK1, MNX1*), δ (*SST, LY6H, SYT1, HHEX*) and γ (*PPY, ETV1, MEIS2, ID2, AQP3*) and confirmed surrogacy for islet transcriptomics in S6w1 islets in comparison to adult islets (Fig. 4f). Specifically, comparison between S6w1 islets *versus* adult islets confirmed the presence of β cell sub populations (β cell and β-like cells) in clusters- 0, 1, and 3 of S6w1 islets; α cell transcripts to clusters- 0, 1 and 6; only a single cluster-7 showed δ-like markers while γ transcripts were attributed to clusters-8 (Fig. 4f).

We next outlined the distribution of β cell functional maturation marker- *PCSK1* attributed to each cluster identified and aligned to *INS* expression. *PCSK1* expression in each identified cluster- matched to those labeled in adult islet datasets, indicating SC-β cell maturation in clusters- 0, 1, 7, and 9 of both S6w1and adult islets. This was consistent with *INS* expression in S6w1 islets, as mature β cells were annotated to clusters 0 and 1. However, we observed lack of *PSCK1* transcripts in cluster-3 of S6w1 islet, despite increased *INS* expression, cells, indicating absence of secretory β cells in this cluster of S6w1 islets compared to donor islets. (Fig. 4g). This was further confirmed with *MNX1, HOPX, MAFA*, and *G6PC2* expression only limited to clusters- 0,1 (Supplementary Fig. 6a–h). Additionally, we observed the expression for SC- α- *GCG* and *ARX* measured in each of these clusters, confirming α cell identity in cluster- 6 like adult islets (Supplementary Fig. 6a–h). Furthermore, violin plot for canonical makers expression of insulin secretion pathway- *CACNA1D, FXYD2, PCSK1N, CHGB, CAMK2N1, PTPRN, HADH, TTR*, and *KCNK3* showed comparable gene expression between S6w1 islets and adult islets. We found no significant difference in OXPHOS associated genes- *MT-CO1, MT-ATP6*, and *MT-ND3* between S6w1 and adult islets, confirming that optimal mitochondrial metabolic maturity is achieved (Fig. 4h).

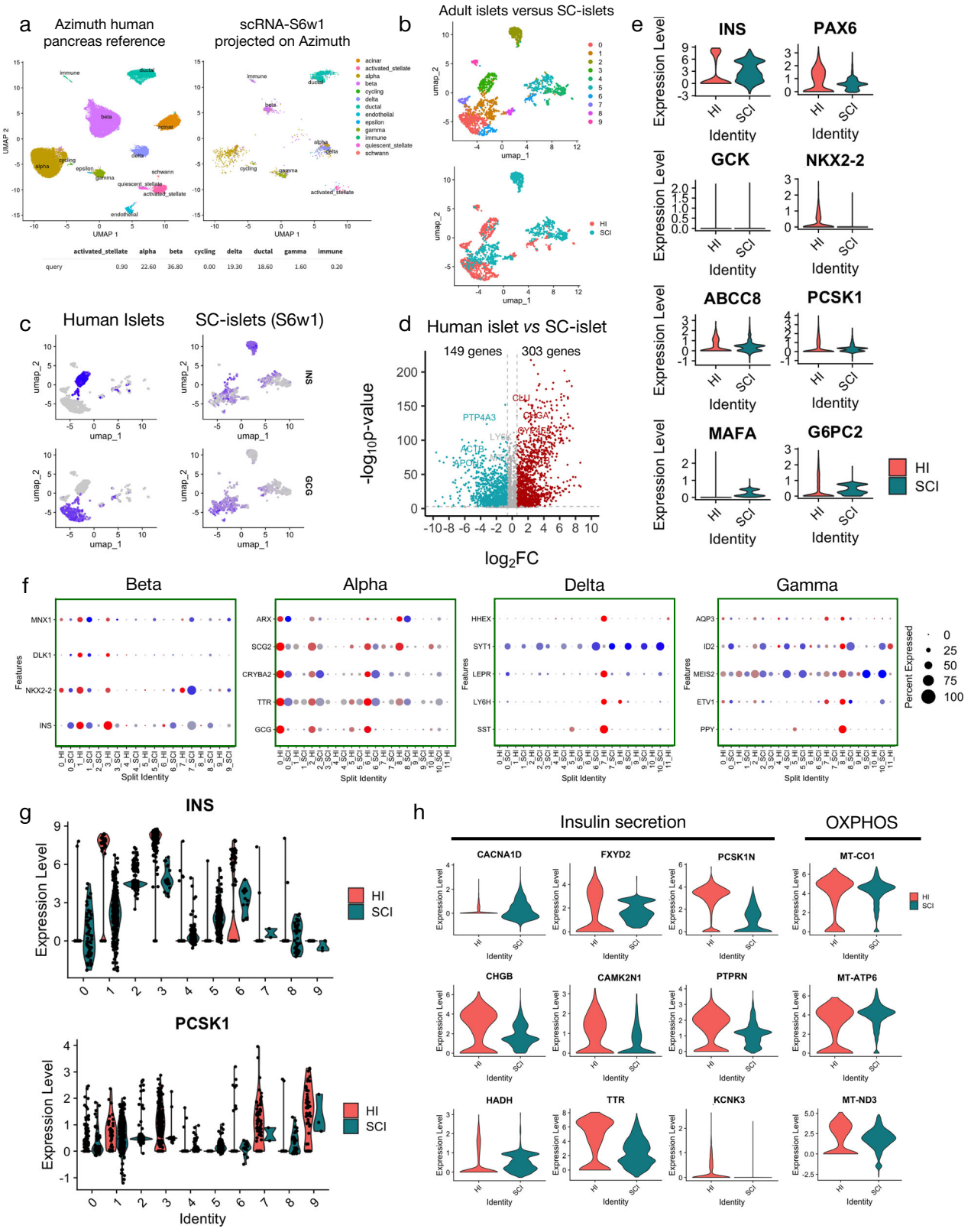

SC-islets exhibit islet developmental and functional maturation without off-target identity

To assess the non-endocrine heterogeneity and immaturity for off-target trajectory, we performed an unsupervised clustering to unveil unbiased projections according to origin and identity. Entire dataset of 17,393 S6w1 cells were clustered into 16 individual clusters (Fig. 5a). After pre-processing QC, a total of 13,442 cells were then classified on unsupervised unimodal UMAP projection. The cell types were annotated as 27% β-like (3572 cells), 10% α -like (1364 cells), and <1% δ -like (153 cells) and γ-like (53 cells) markers, based on the canonical marker surveillance for individual islet cell population as described in Azimuth reference[42–50]. A total of 16% cells were observed with endothelial (2193 cells), 3% endocrine

Fig. 4 | Comparative characterization of S6w1 scRNAseq dataset with Azimuth human pancreas reference and donor islets. a Azimuth UMAP- base embedding projection to identify human pancreatic islet cell populations clustered from S6w1 scRNAseq datasets ($n = 2$ batches from a healthy iPSC line, 17,393 cells) after annotating with reference human pancreas dataset- Satija lab https://azimuth.hubmapconsortium.org/references/human_pancreas/ (GSE217837; $n = 3$ donors, 35,289 cells). **b** UMAP projection representing total 9 clusters identified between S6w1 SC-islets and donor adult islets using RStudio v2023.06.2 + 561 and Seurat v4.3.2. **c** Feature plots representing INS and GCG expression in identified clusters between S6w1 SC-islets and adult islets. **d** Volcano plot to show differentially expressed genes in S6w1 islet dataset in comparison to donor islets. Genes in red show upregulated genes and in cyan downregulated genes. **e** Violin plots to show comparative gene expression for key β cell specific markers between S6w1 islets and adult islets. Expression values on y-axis are shown as z-score normalized data for each gene. **f** Feature dot plots displaying representative markers for SC- β, -α, -δ, and -γ cells on individual clusters identified between islets and adult islets. Red color dots denote human donor islets and blue corresponds to S6w1 islets clusters. The size of the dots denotes counts expressing these features matched to the scale (0–100%) **g** Violin plots showing comparative gene expression distribution for *INS* and *PCSK1* in individual cluster between S6w1 islets and donor islets. **h** Violin plots comparing gene expression levels for insulin secretion and OXPHOS associated genes between S6w1 islets and donor islets. Expression values on y-axis are shown as z-score normalized data for each gene.

(436 cells), and 9% duct-like (1225 cells) markers (Fig. 5a Supplementary Fig. 2e).

We specifically resolved the clustering of S6w1 islets generated from 0.1 L and moving to scale-up 0.5 L vessels to delineate the cellular heterogeneity. We observed no difference between the 2x replicate testing as SC-islets showed defined and identical clustering of RNA transcripts on UMAP projections (Fig. 5b). Feature plot projection focused specifically on endocrine clusters revealed marked expression for *INS, PCSK1, NKX6-1, GLIS3, CD81*, and *HOPX* genes on SC-β-like cluster only, while *MAFA* and *SIX2* were moderately expressed, confirming an established β-cell identity, as observed in mature β-cells. (Fig. 5c). Comprehensive evaluation of islet-specific gene transcripts across all endocrine clusters suggested demonstrated high expression for islet developmental genes, including *PDX1, NKX6-1, INS, GCG, SST, PPY, GHRL, GLP1R, CHGA, MNX1, ARX, HHEX, TSPAN8*, and *KRT20* (Fig. 5d). Here, β-cell specific cluster showed expression for *INS* combined with *MNX1, PDX1, NKX6-1*, and *GLP1R*, while *GCG* expressing cluster only expressed *ARX*, confirming SC-β and - α cell identity, respectively. Other islet hormonal cells- SC-δ, SC-γ, and SC-ε cells showed minimal lineage specific expression for *HHEX, TSPAN8*, and *KRT20*, respectively. (Fig. 5d).

We generated heatmap plots to evaluate islet development genes expression across identified endocrine clusters (Fig. 5e). Expression level was graded using a color intensity gradient, where significantly upregulated genes were scored in red and repressed genes scored in blue. As expected, cluster annotated for SC-β showed upregulation for maturation associated genes, including *GLP1R, PAX4, KCNJ3, MNX1, NKX2-2, CHGB, PCSK1*, and *NKX6-1*. Similarly, clusters for SC-α cell annotation had distinct set of transcript upregulation- *GCG, ARX, PPY, ISL1, SST, GHRL, CHGA, INS, NEUROD1*, and *PDX1*. Contrastingly, non-endocrine cells, ductal and endocrine annotated clusters showed downregulation of the above genes (Fig. 5e). The top 100 differentially expressed genes between identified endocrine-specific clusters are shown in Supplementary Fig. 2g.

Our evaluation for functional islet genes to clearly discern functional transcriptomic architecture of clusters across different islet cell populations allowed mapping endocrine rich genes using violin plots. Specifically, we compared SC-β, SC-α, Polyhormonal (SC-PH), and endocrine population for genes- *MAFA, NKX6-1, MNX1, ARX, CD81, GLIS3, PCSK1, HOPX, GLP-1R, KCNJ3*, and *SLC30A8*. In S6w1 cells, canonical marker *INS* was profoundly expressed in both SC-β and SC-α annotated cluster, while *MAFA* was only modestly expressed. Similarly, *NKX6.1* and *MNX1* were expressed by SC-β annotated cluster comparted to *CD81* and *GLIS3*- genes for insulin secretion regulation, those expressed across endocrine cell populations. The presence of insulin secretion transcriptomic machinery (*PCSK1*, *HOPX, GLP1R, KXNJ3*, and *SLC30A8*) was prominently expressed only in SC-β annotated cluster, highlighting functional maturity of S6w1 cells (Fig. 5f).

Next, we compared the transcriptomic footprints for glycolysis and TCA cycle pathway, insulin secretion machinery, exocytosis and disallowed genes between unsupervised endocrine clusters to ascertain their functional maturity in individually annotated clusters. Dot plot resolution for an absolute gene expression in each of these clusters outlined in-vitro functional maturation exhibited to SC-β cluster amongst all other clusters. Most SC-β clusters and other clusters expressed glycolysis and TCA metabolism genes- PFKL, SLC2A1, SLC25A1, SUCLG2, while other genes- *G6PC2, FBP1, GPD1, GCK*, and *SLC2A2* were minimally expressed (Fig. 5f). Although, SC-β cluster was found enriched in a few glycolysis and TCA enzyme coding gene- *PFKL, SLC25A1, GDP1*, and *GCK*, other crucial transcripts- *G2PC2, FBP1, GPD1*, and *SLC2A2* was mildly expressed, suggesting in-vitro ongoing functional maturity and require further maturation. Contrastingly, SC-EC cells did not express any of glycolysis and TCA genes, suggesting serotonin secretory cells are not β-like cells (Fig. 5g). We then investigated key markers for insulin secretion cascade- *PCSK1, CAMK2N1, GRN, TTR, CHGB, PTPRN, FXYD2, CASR, KCNK3, KCNJ3, CACNA1D*, and *HADH*. Here, particularly, SC-β cluster represented marked expression for majority of insulin secretory genes, while other clusters- SC-α, and SC-PH minimally expressed genes (Fig. 5h). With respect to exocytosis genes, SC-β cluster exhibited presence of exocytotic genes- STX4, STX3, RAB27A, and STXBP5L, suggesting SC-β cells attained both secretion and exocytotic capacity (Fig. 5i).

We further investigated transcriptional identity of disallowed and off-target lineage genes. In prior studies, important "disallowed" genes have been identified in pancreatic islets - upregulation of these genes can impede glucose-regulated insulin secretion[52]. Reassuringly, our S6w1 generated SC-islets had minimal expression of most disallowed genes, *LDHB, HK2, HK1*, and *SLC16A1* but with a moderate expression for *LDHA* (Fig. 5j). Other clusters representing duct, SC-δ, SC-γ, and SC-ε showed expression for disallowed genes (Fig. 5j, k). As final evaluation of our cell product, we noted downregulation for off-target gene expression in feature plots for *POU5F1, PLK1*, with minimal *MKI67* expression (Fig. 5k). We systematically evaluated and characterized off target genes associated with pluripotency, cancer and metastatic, cell proliferation and metabolism pathways and, tri-lineage and immune recognition genes. Dot plot representation of canonical genes regulating non-pancreatic pathways suggested the purity and mitigation for contaminating off-target cells within our suspension generated SC-islets. Pluripotency associated genes- *POU5F1, SOX2*, and *MYC* were confirmed downregulated and absent among all identified clusters. Additionally, transcripts expressed in cancer, metastasis and cell invasion were also not expressed. Importantly, among all transcriptomic clusters except for SC-EC, we observed a variable level of gene upregulation for cell proliferation, cell adhesion and metabolic pathway genes (Supplementary Fig. 2f).

Several studies suggest that ectoderm-derived neurons and endoderm-derived β cells share close developmental pathways. During differentiation β cells share nearly 15% of conserved markers with neuronal cells[53]. In our own datasets, we noticed all clusters, including SC-β, expressing neural lineage genes- *SOX11, FOXJ1*, and *MAP1B*, indicating that SC-islets and neuronal cells may be predominantly derived from similar progenitors. Furthermore, S6w1 single cell datasets showed downregulation of mesoderm or early foregut endoderm genes that produce cardiac, osteo, cartilage, adipose, and intestinal lineage cells, supporting the prevention of off-target cell population formation. Finally, all clusters were detected expressing markers for pancreatic endocrine and exocrine cells, as well as immune cells, suggesting that S6w1 cells differentiated only to pancreatic linage and share immune recognition footprints. (Supplementary Fig. 2f).

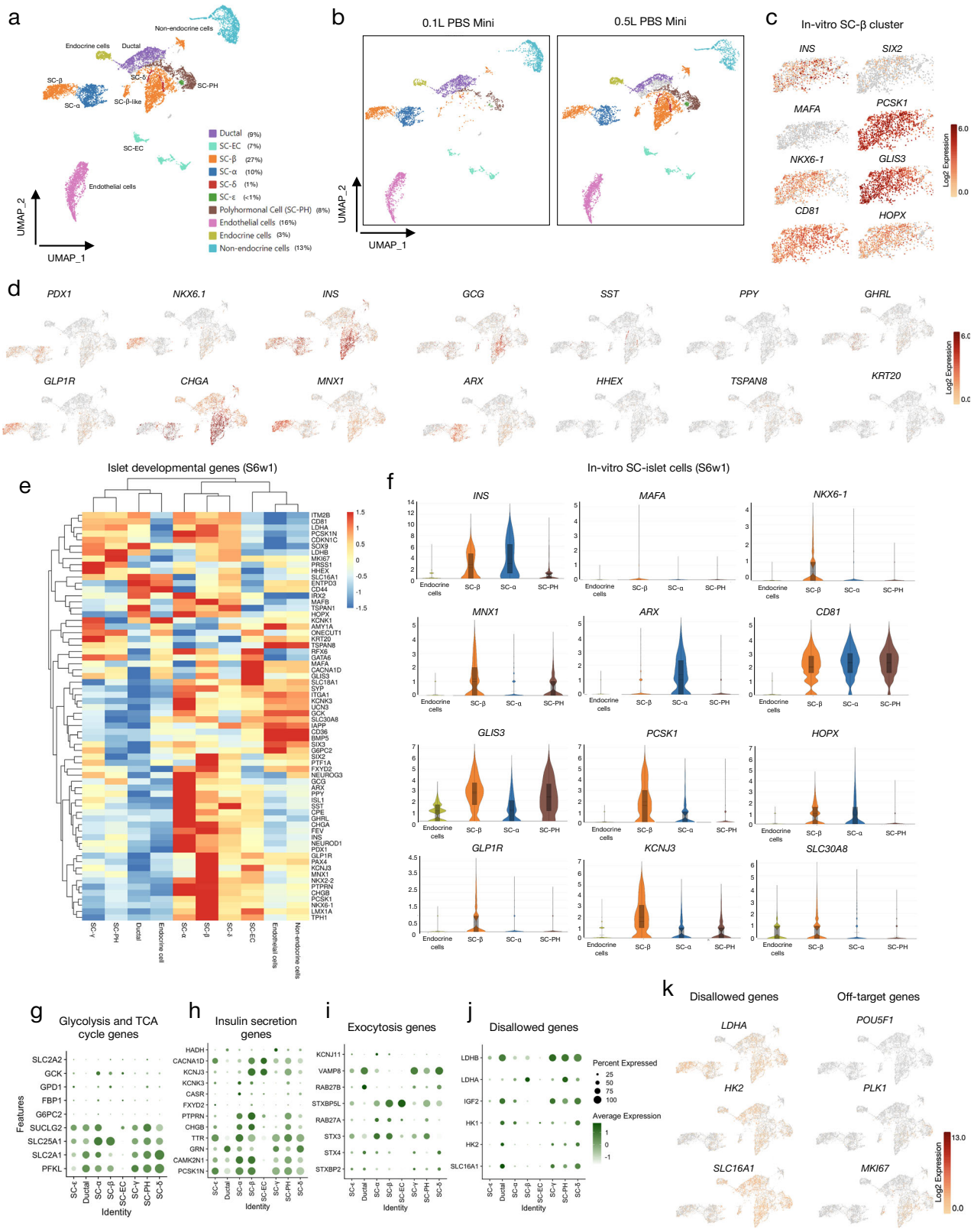

Suspension SC-islets are transcriptionally comparable to other SC-islet datasets

We then focused on comparing the transcriptional maturation of our S6w1 transcriptomic datasets to previously published SC-islet datasets. Recently, several groups have shown approaches for generating efficient production of functional SC-islets from human embryonic stem cells[5,11,12,14–16,21,39,54,55]. Three major reports from Veres. et al.[14], Augsornworawat et al.[56], and Balboa et al.[12] compared SC-islet genomic architectures in-vitro and characterized SC-islets to compare the efficiency of cell production methods and described a comprehensive primary classification of makers to resolute cellular identity and transcriptomic maturation of SC-islets. For transcriptionally comparing our S6w1 islet dataset with published SC-islets datasets, we

Fig. 5 | Unsupervised characterization of identified clusters from S6w1 scRNAseq dataset. a UMAP projection of combined two samples of S6w1 islets from a healthy iPSC line representing annotated islet cell population guided through islet development feature expression without reference dataset supervision. Samples were analyzed using 10X genomics software Loupe Browser v7.0.01. Clusters identified and annotated for frequency distribution as- SC- β (27%), SC-α (10%), SC-δ (1%), SC-γ (<1%), ductal (9%), SC-EC (7%), SC-polyhormonal (8%), Endothelial cells (16%), Endocrine cells (3%), non-endocrine cells (13%). **b** Comparative cluster identification of each sample obtained from 0.1 L and scale-up 0.5 L generated S6w1 islets to show in UMAP projection and liberality of differentiation without variability. **c** Feature plots of SC- β cell cluster highlighting functional β cell marker expression. Scale represents log2FC expression (0–6). Color highlight as pale yellow: downregulation and crimson red: upregulation. **d** Feature plots of selected endocrine clusters representing expression for islet cell differentiation and exocrine markers. Scale represents log2FC expression (0–6). Color highlight as pale yellow: downregulation and crimson red: upregulation. **e** Heat map plot with Manhattan neighbor distribution clustering representing differentially expressed genes associated with islet developmental pathway between identified and unsupervised annotated clusters. Scale represents log2FC (−1.5 to 1.5), where red color shows upregulation and blue corresponds to downregulation of selected gene expression. **f**, Violin plots comparing distribution of β and α cell makers for functional maturation gene expression between SC- β, -α, -PH, and endocrine cells. Each plot shows median gene expression distribution with interquartile range for 27–75%. **g** Dot plot representing differentially expressed genes for glycolysis and TCA metabolism, **h** Dot plot representing differentially expressed genes for insulin secretion, **i** Dot plot representing differentially expressed genes for exocytosis, and **j** Dot plot representing differentially expressed genes for disallowed genes between SC- β, -α, -δ -γ, -ε, -PH, -EC, and ductal cells. **k** Feature plots of endocrine clusters representing disallowed and off-target pluripotency associated genes expression. Scale represents log2FC expression (0–13). Color highlight as pale yellow: least expression and crimson red: upregulation, gray represents absence of gene expression.

obtained scRNAseq datasets from Balboa et al. (GSE167880)[12] and Augsornworawat et al. (GSE139535)[56] as reference datasets.

First, we combined and merged the filtered and processed datasets from our S6w1 islets, final stage product from Balboa et al., and Augsornworawat et al. UMAP projection. We observed a distinct separation of clusters with few equivalent populations clustered together with our dataset. Compared to Balboa et al., cells from our S6w1 clustered in 0, 4, and 5 clusters while an overlap of clusters- 1, 3, 5, 6 and 7 was observed with Augsornworawat et al. dataset (Fig. 6a). In comparison to Balboa et al. we identified 0, 1, 4, 5, and 6 as equivalent clusters, while our dataset also contained another population that clustered separately, as indicated in cluster- 2 (completely absent in the Balboa et al. dataset). Interestingly in comparison to Augsornworawat et al. dataset, we noticed the existence of clusters- 1, 3, 4, 5, and 6 in both datasets, however our dataset contained another cluster- 2 which was absent in Augsornworawat et al. dataset, similar to Balboa et al. (Fig. 6b). We therefore compared DEG and investigated canonical islet makers to compare the existence of each islet cell population between our dataset and others.

We plotted overall gene expression of all identified clusters discovered between our S6w1 dataset and final products from Balboa et al. and Augsornworawat et al. as volcano plots. We found 1466 genes were downregulated and 1281 genes upregulated in our S6w1 islets compared to Balboa et al. Similarly, we discovered downregulation for 1192 genes and overexpression for 1730 genes in our dataset compared to Augsornworawat et al. SC-islets. (Fig. 6c). Upon comparing SC-β and -α clusters DGE, specifically between the three data sets, we noticed 241 genes were downregulated in our S6w1 SC-β, while 157 genes were upregulated in Balboa et al. SC-β. Likewise, 156 genes were downregulated in S6w1 SC- α, while Balboa et al. SC- α showed an increase of 170 genes.

Compared to Augsornworawat et al. dataset, S6w1 SC-β exhibited downregulation for 58 genes and overexpression for 48 genes in Augsornworawat et al. SC-β, while downregulation for 330 genes in S6w1 α cluster was observed compared to 321 genes upregulation in Augsornworawat et al. SC-α cluster. (Fig. 6d). Dot plot comparison presents each of these clusters in direct evaluation for SC-β, SC- α, SC-δ, and SC-γ identity. For SC-β, we found clusters- 1, 4 and 5 coincide equivalents to Balboa et al. dataset while clusters- 0, 3 and 4 matches with Augsornworawat et al. dataset for β- cell identity markers- *INS, NKX2-2, DLK1*, and *MNX1*. Similarly, we found clusters 0 and 4 showed α- cell identity markers- *GCG, TTR, CRYBA2, SCG2*, and *ARX* in S6w1 dataset compared to both Balboa et al. and Augsornworawat et al. datasets. Additionally, our datasets align for SC-δ, and SC-γ identity on a single cluster compared to both datasets (Fig. 6e).

We then assessed and compared an absolute transcript level for endocrine islet cell identity-*INS, GCG, SST, PPY*, and *GHRL* between S6w1 *versus* Balboa et al. and Augsornworawat et al. datasets. Balboa SC-islets demonstrated bimodal expression for both *INS* and *GCG*, as seen in adult donor islets. Our S6w1 dataset, however, demonstrated bimodal expression but modestly with low distribution for high *INS* transcripts. Likewise, Augsornworawat et al. SC-islets also showed high *INS* and *GCG* bimodal transcripts compared to our SC-islet transcripts. Collectively, in comparison to both datasets our S6w1 SC-islets show some level for immaturity within the 27 days of differentiation. For SST expression, we observed a higher SST transcript level in comparison. Both Balboa et al. and Augsornworawat et al. showed minimal transcript levels for *PPY* and *GHRL* transcripts, while S6w1 islets showed higher transcript levels (Fig. 6f). We compared several markers for β-cell identity, metabolism, and disallowed genes, in comparison to datasets from two published studies, these are detailed in Supplementary Fig 7a–c. Finally, we also represented key islet markers for all islet populations on feature plots to effectively compare and identify SC-β, SC- α, SC-δ, and SC-γ populations on UMAP projections. In comparison to both published datasets, S6w1 SC-islets showed presence of all islet cell identity markers and resonated for SC-islet heterogeneity and cell composition (Fig. 6g). More details are summarized in Supplementary Fig. 7d. Taken together, we observed a comparable resolution of detailed transcriptional maturation markers in SC-islet development and differentiation, and we believe that our data corroborate that published datasets as we move our process for scale up.

SC-progenitors and SC-islets exhibit single cell dimensionality reduction and islet phenotype

Further, mass flow cytometry provides a unique opportunity to interrogate large numbers of cells with multiple parameters at the single-cell level in parallel, thus facilitating identification of rare cell types and subtype-specific behavior[57,58]. We performed high-dimensional single-cell data visualization using machine learning approach. We generated multiplex flow data with accutase-dispersed single cells stained with a panel of stage-4 (pancreatic progenitor) and stage-6 (islets) antibodies (Fig. 7a). Utilizing viSNE plots, we created a high-dimensional single-cell data visualization based on the t-Distributed Stochastic Neighbor Embedding (t-SNE) algorithm from SC-derived S4 and S6 cells. viSNE helped in determining the best 2D representation of the single-cell mass flow cytometry data in terms of local and global geometry from pancreatic progenitors versus differentiated SC-islet cells. We compared cellular composition and underlying heterogeneity between SC-derived S4 cells, S6 cells compared to adult donor islets.

Mass flow cytometry viSNE analysis from 50,000 cells revealed that we were able to obtain a single-cell high resolution map of cellular heterogeneity between S4 and S6 cells by multiplexing antibodies cocktail (S4: PDX1, NKX6.1, GP2, CHGA; and S6: INS, GCG, SST, CPPT, NKX6.1, ISL1). First, we marked and compared pancreatic progenitor markers- PDX1, NKX6.1, GP2, and CHGA expression on S4 single-cells to resolute pancreatic progenitor cell heterogeneity during S4 differentiation. viSNE single cell island geometry of S4 cells demonstrated comparable and unified expression of PDX1, NKX6.1, and CHGA similar to adult islets (Fig. 7b). We compared the expression of S4 markers using 3 donor iPSC lines after independent batches of S4

differentiation against representative cadaveric islets for stochastic distribution for pancreatic progenitor markers- PDX1, NKX6.1 and complemented with pan endocrine tracer- CHGA expression (Fig. 7b; Supplementary Fig. 8a). Here, the intensity color spectrum (blue-low to red-high) characterized the average expression for each marker on each cell that are clustered in viSNE island, depicting relationship between clusters and heterogeneity.

viSNE single cell island geometry of S4 cells demonstrated absolute transition of homogeneous PDX1 and NKX6.1 expressing population in yellow to red, that are weakly and uniformly CHGA positive (cyan). Here,

Fig. 6 | Single cell transcriptomic comparison of SC-islets with published SC-islet datasets. a UMAP-base embedding overlay projections (Seurat v4.3.2.) indicating SC-islet transcriptomic comparison across healthy iPSC-derived S6w1 islets from Dadheech et al. (current study) with filtered and preprocessed feature matrix counts from Balboa et al. (S7w0- GSE167880) and Punn et al. (S6- GSE139535). **b** UMAP projection depicting cluster identification between Dadheech et al. *versus* Balboa et al. (0,1,2,3,4,5,6 clusters) and Dadheech et al. *versus* Punn et al. (0,1,2,3,4,5,6,7 clusters) datasets. **c** Volcano plots indicating differentially expressed genes among each cluster in comparison between Dadheech et al. *versus* Balboa et al. and Dadheech et al. *versus* Punn et al. datasets. Genes in red show upregulated genes and in cyan downregulated genes. **d** Volcano plots indicating differentially expressed genes after comparing β and α clusters only between Dadheech et al. *versus* Balboa et al. and Dadheech et al. *versus* Punn et al. datasets. Genes in red show upregulated genes and in cyan downregulated genes. **e** Feature dot plots displaying representative markers for SC- β, -α, -δ, and -γ cells on individual clusters identified between Dadheech et al. *versus* Balboa et al. and Dadheech et al. *versus* Punn et al. datasets. Red color dots denote Balboa et al. or Punn et al. datasets and blue correspond to S6w1 islet dataset. The size of the dots denotes counts expressing these features matched to the scale (0-100%). **f** Violin plots showing comparative gene expression distribution for representative islet population markers- *INS, GCG, SST, PPY*, and *GHRL* in S6w1 islet dataset in comparison to published Balboa et al. and Punn et al. SC-islet datasets. Expression values on y-axis are shown as z-score normalized data for each gene. **g** Feature plot indicating distribution of *INS* expression in S6w1 islet dataset *versus* Balboa et al. and Punn et al. datasets.

the undifferentiated control cells as clustered in a single blue population depicted negative PDX1 and NKX6.1 expression and clustered separately from pancreatic progenitor cell island. This data collectively demonstrating efficient transition of S4 cells expressing PDX1 and NKX6.1 dual positive cells as pancreatic progenitors (Fig. 7b). This was further confirmed, immunohistochemically, with nuclear PDX1 (green), NKX6.1 (red), with cytoplasmic GP2 (red) staining in S4 clusters (Fig. 7b). Together, our data suggest that suspension generated S4 product demonstrate a strongly cohesive and homogenous pancreatic PDX1$^+$ progenitor population that also exhibiting GP2$^+$ and NKX6.1$^+$ expression with minimal frequency of CHGA co-expression.

We then analyzed the multiplexed flow data using FlowSOM tool that draw lineage trajectory of single-cell clusters that corresponds to well separated progenitor cell population and the subsets of endocrine islet populations. FlowSOM output, which concatenates the mass flow cytometry data, generated self-organizing maps to visualize clustering and dimensionality reduction. The approach has an advantage of providing a comprehensive overview of each marker's expression level at single cell resolution and the potential to identify unsupervised cell populations undergoing pancreatic lineage trajectory. Using S4 multiplex data, the individual heatmaps that are projected onto the self-organizing maps for each marker demonstrating the expression level for each progenitor marker in all corresponding cell subpopulations (Supplementary Fig. 8a).

Evidently, NKX6.1 was profoundly expressed (yellow to red) in majority of S4 cells, medium in donor islets (cyan to green) and were absent (blue) in undifferentiated control. Moreover, combined detected of high NKX6.1$^+$CHGA$^-$ and heterogeneous PDX1$^+$GP2$^+$ expression was identified across all cell subpopulation of S4 clusters, suggesting S4 cells are minimally heterogeneous (Fig. 7c). Notably, the extent of pancreatic progenitor population within the suspension differentiation of S4 clusters was pronounced as S4- PDX1$^+$NKX6$^+$CHGA$^-$ in self-organizing- Star Plot maps (Supplementary Fig. 8b), confirming efficient S4 cell generation within the bioreactors.

We then utilized similar approach to map out heterogeneity and composition between S6w1 islets, donor islets, and undifferentiated control (Fig. 4a). Here, the panel of antibodies used clearly resolved endocrine cell populations. SC-islet cells exhibited intense and uniform NKX6.1 and CHGA expressing population, distributed across all viSNE island, similar to adult islets (Fig. 7d). Moreover, self-organizing map (Star plots) of S6w1 cells showed three distinct meta clusters- GCG$^+$, INS$^+$, and SST$^+$, similar to donor islets (Supplementary Fig. 9b). A high-dimensional single-cell analysis of islet hormones expression revealed that SC-islets had undergone endocrine (islet) reprogramming. We gated endocrine subtypes in SC-islet clusters using viSNE plots to mark the hormone-expressing cells and compared against primary islets.

To validate the map, we used an independently derived classification of S6 cells to islet subtypes, based on manual gating of a series of biaxial plots (see "Materials and Methods"). Notably, our method defined INS$^+$ β cells formed as distinct islet subset in the viSNE island and remained distinct from GCG$^+$ α and SST+ δ cells (Supplementary Fig. 9b). While viSNE plots are not provided with detailed annotated classification or any knowledge of endocrine *versus* non-endocrine subsets by default, it grouped the cells in the same subsets together and separated from one another based on distribution of probed islet-endocrine markers. Applying manual gating to mark populations showing high expression for S6 marker, we transferred annotations for each subpopulation on viSNE plots. Following manual annotations, viSNE accurately distinguished NKX6.1$^+$ and CHGA$^+$ cells (62.90%; IQR: 67.80–56.65% and 57.75%; IQR: 63.0–48.75%; $n = 4$, respectively) as mature endocrine cells in S6 compared to adult islets (Supplementary fig. 9c).

Lastly, we performed viSNE analysis on SC-islets to exclusively gate for β cells using surrogate antibody for gold standard β cell markers- CPPT, NKX6.1, and ISL1. This process confirmed the presence of true β cells within the SC-islet populations. Using spectral maps as a guide, we hand-delineated β cells cluster to further detect for co-expression with NKX6.1 and ISL1 (Fig. 7d). We performed a number of analyses to evaluate the robustness of viSNE classification. The viSNE map included 10,000 cells that were subsampled from the complete data set (each for iPSC, -S4, -S6 and donor islets). We independently subsampled multiple subsets of the data and ran FLOWSOM on each sample, resulting in similar FLOWSOM plots that conserve the separation across all subsets (Fig. 7d; Supplementary Fig. 9a) This supports the notion that the viSNE map is consistent and reliable in representing an ideal islet heterogeneity.

In parallel, immunohistochemical staining for β cell-specific markers-CPPT (green), NKX6.1 (red), and ISL1(red) endorsed islet differentiation in SC-islets under suspension bioreactors (Fig. 7d). To test islet-specific heterogeneity, we performed population trajectory meta cluster analysis in self-organizing maps- (Star Plots) from S6 cells. We observed comparable lineage distribution for islet populations expressing- INS, GCG, and SST. Further, specifically, INS$^+$ cluster in Star plot show linear correlation with the presence of β cell identity markers- CPPT, NKX6.1, and ISL1 (Supplementary Fig. 9b). Remarkably, minimal spreading of β subpopulation in the self-organizing maps reflected controlled cellular heterogeneity within the SC-islet cell composition.

Discussion

Human PSCs offer promise for the generation of stem cell-derived islets for diabetes cell therapy[10,26]. However, scaling up the manufacturing process without pooling of multiple preparations remains a challenge for clinical application, and will be important if a consistent, functional SC-islet product is to be made[4,31]. Various methods, including small to mid-size planar or suspension culture formats like ultra-low attachment or microwell plates, and spinner flasks, have been explored to scale SC-islets production[10,14,28–30,59]. Despite these advances, such approaches are generally suitable for the generation of only limited number of islet equivalents, primarily at research scale. A major research focus is enhancing the manufacture of transplantable mass of islet equivalents in a single batch. Cell loss, batch-to-batch variability, and off-target heterogeneity together with cost containment remain crucial considerations if such therapies are to become routine in the clinic.

Suspension bioreactors present one potential solution for scale-up manufacture. Current technologies face limitations in GMP manufacturing, primarily due to equipment compliance, cell loss, and validation of process control. Spinner flask bioreactors, with capacities ranging from 30 to 500 ml, have been documented to generate SC-islets from human embryonic stem

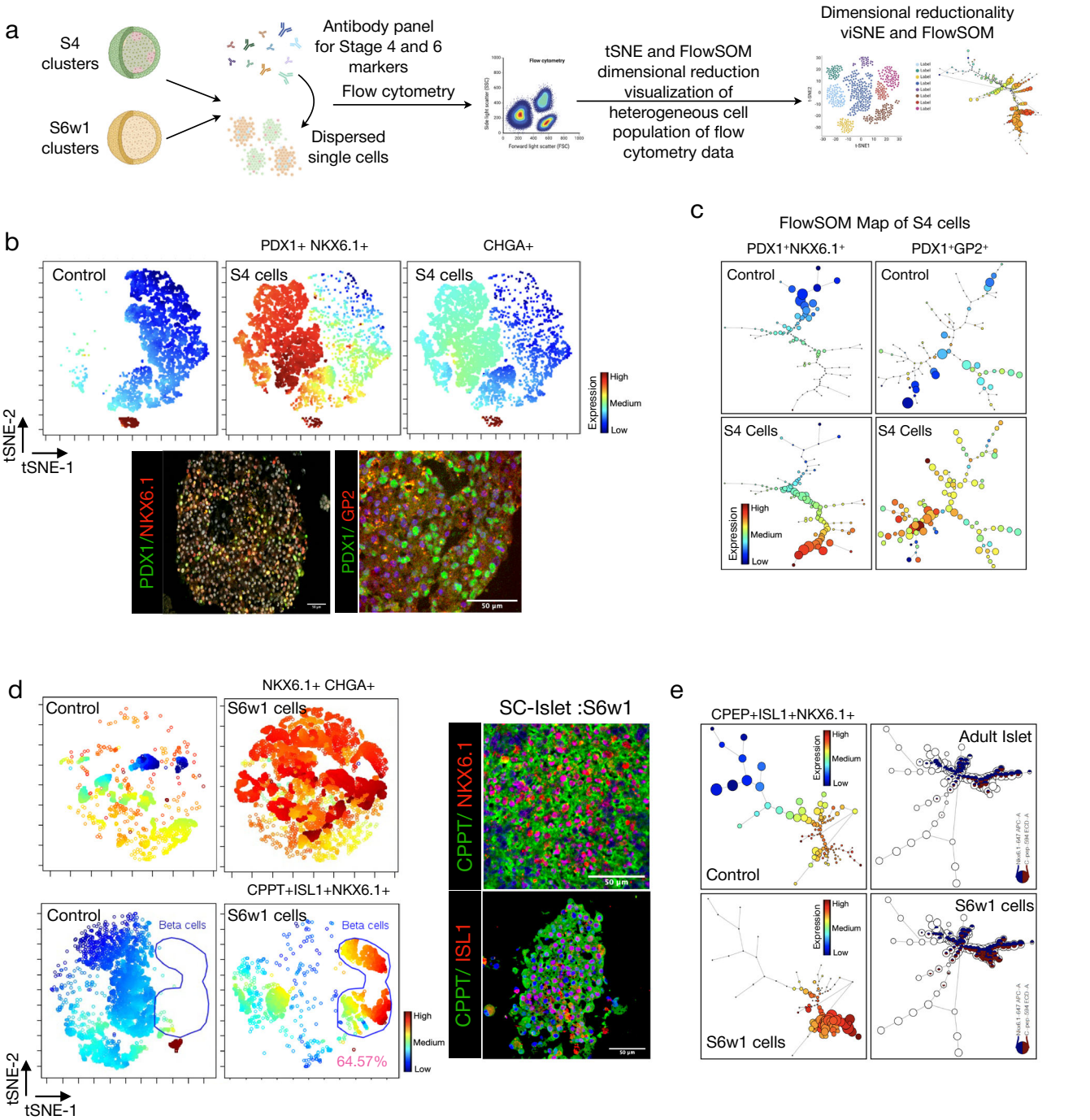

Fig. 7 | Dimensionality reductional visualization for cellular heterogeneity in pancreatic progenitor and SC-islets. a Experimental overview of single cells flow cytometry and dimensionality reductional analysis in S4 cells and S6 islets generated from healthy, total pancreatectomy, and type-1 diabetes donor iPSC lines. Created in BioRender. Dadheech, N. (2025) https://BioRender.com/u86j668. **b** viSNE visualization of 50,000 stage-4 progenitor cells for PDX1, NKX6.1, and CHGA markers against undifferentiated control. Color gradient represents the marker expression density in each cell from high (red) to low (blue) distributed in a viSNE islands. Immunohistochemistry of S4 cluster indicating staining for PDX1- (green), NKX6.1, and GP2 (red). Scale bars, 50 µm. **c** Self-organizing map (FlowSOM) dimensionality reductional visualization of S4 pancreatic progenitor cells for PDX1, NKX6.1, GP2 markers against undifferentiated control. Color gradient represents the density of marker expression density in each cell from high (red) to low (blue) to show heterogeneity in endocrine lineage trajectory. **d** viSNE visualization of 50,000 S6w1 cells for CPPT, ISL1, NKX6.1 and CHGA against undifferentiated control. Color scale represents the marker expression density in each cell from high (red) to low (blue) distributed in a viSNE islands. Immunohistochemistry of S6w1 cluster indicating staining for CPPT- (green), NKX6.1, and ISL1 (red). Scale bars, 50 µm. **e** Self-organizing map (FlowSOM) dimensionality reductional visualization of S6w1 islet cells for CPPT, ISL1, and NKX6.1 markers against adult islets as control. Color gradient represents the density of marker expression density in each cell from high (red) to low (blue) to show heterogeneity in endocrine lineage trajectory. Single cell flow cytometry datasets were analyzed using Cytobank Premium software v10.6 https://premium.cytobank.org/cytobank/.

cells in full suspension culture[14,28,29]. However, cell yield and cell loss remain compromised due to damage from fluid dynamics and physical sheer. PBS mini-Vertical Wheel® bioreactors have recently shown promise in commercial scale-up PSC-derived products[60]. These GMP-compliant bioreactors provide a highly controlled, low-shear, and dynamic 3D microenvironment for stem cell growth and directed differentiation into multiple tissue lineages[38,61,62]. Computational bioengineering studies comparing fluid dynamic models suggest that PBS bioreactors are favorable for stem cell expansion and scale-up, with minimal cell loss[60,61].

Recent advancements in SC-islet generation protocols using planar (2D) or 3D suspension conditions, are capable of generating mature islet-like products, albeit with limited yield. Using the planar approach, Balboa et al. and Barsby et al. have generated 8000–10,000 functional SC-islet clusters at S6-S7 stages from a combined pool of two confluent 10 cm dishes harvested, totaling 36×10^6 pancreatic progenitor cell population[12,63]. Similarly, Hogrebe and colleagues employed both planar (T-75) and suspension (30 ml spinner flask) approaches, reporting the production of 340–750 million SC-β-cells by combining multiple (6–13) standard T-75 flasks[11]. While these procedures are scalable, the requirement for numerous cell culture units, along with labor-intensive manpower for cell processing, could introduce batch-to-batch variability and risk of contamination upon vessel pooling. Consequently, this practice renders the manufacturing process costly and challenging for scale-up within the context of a cGMP manufacturing environment.

In the current study, we describe a modified 3D suspension islet differentiation protocol for human iPSC expansion and islet differentiation within PBS VW® bioreactors (Fig. 1a). The approach is reproducible and scalable, capable of generating high numbers and IEQs of SC-islets without alteration in morphology, size, or off-target heterogeneity (Fig. 1c). The protocol is scalable, uses low-shear bioreactor technology that is capable of 5x scale-up from 0.1 L to 0.5 L capacity without need for disaggregation-reaggregation, as previously described in other protocols[11,13–16,63] (Supplementary Material Table S8). We consistently achieve a median yield of 28,050 to 61,083 SC-islets, corresponding to over a 12-fold increase in (15,005-183,002) IEQ generation when transitioning from 0.1 L to the scaled-up 0.5 L volume (5 times vessel size) (Fig. 1f). Notably, the scale-up efficiency is linear (without significant change) across the transition from 0.1 L to the scaled-up 0.5 L vessel, producing a median of 0.39 to 0.41 million S6 cells per million iPSCs (Fig. 1d, e). Consequently, this technology renders the manufacturing process highly suitable and scalable under GMP compliance, eliminating batch-to-batch variation. A comparative evaluation of critical parameters and outcomes of key published protocols against the current protocol is summarized in Supplementary Material Table S8. Our data demonstrates a 12-fold increase in SC-islet generation despite only a 5-fold increase in vessel size, permitting linear scale-up without compromise to islet architecture or morphology. Our current protocol is equivalent but not superior to other published protocols in terms of in-vitro functionality and islet maturation. Although the SC-islets (at 27 days) are immature in-vitro, a potential advantage of this current process is scaling of SC-islet production in a short period of time without requirement for destructive physical dissociation. This protocol augments SC-islet production by 12-fold in terms of IEQ within a 0.5 L scale without compromise to cell composition or islet-like architecture, while reducing overall cell loss. A summary of key bioprocess parameters comparing other published protocols is described in Supplementary Material Table S8.

Our complete suspension method shows potential in generating defined endocrine cell populations within 27 days (Fig. 1h–k), exhibiting 51.8 ± 2.3% SC-β cell markers (CPPT+NKX6.1) and mono-hormonal cells expressing INS+, GCG+, INS+MAFA+. Using Aphidicolin (APH) as a small molecule during Stage 6, S6W1 islets demonstrate minimal frequency ~6% of enterochromaffin cells (SC-EC: SLC18A1+/LMX1A+) and non-endocrine lineage markers, indicating that the approach effectively limits and reduces off-target serotonin secretory enterochromaffin cell production during the terminal phases of differentiation (Fig. 1j, k). These findings are consistent with the SC-islet phenotype previously discussed in prominent published protocols utilizing ESCs in both planar[11,12,39,55,63] and suspension conditions[14,28–30]. Although APH has a strong effect on endocrine differentiation and helps minimizing the risk for teratogenic growth from residual proliferating cells, several reports suggest its inhibitory effect on DNA polymerases (delta and epsilon). This effect may impair nuclear excision and DNA repair[64–66] and could inadvertently affect the genomic stability of the final product. Hence, low toxic cell cycle inhibitors such as PD166167[67] and ZM4260[12] should be explored.

Indeed, the S6 islets exhibited glucose responsiveness, secreting insulin in response to varying glucose concentrations and stimulators (Fig. 2a–c). Notably, the bioreactor system facilitated the generation of a large number of uniform and homogeneous SC-islets, demonstrating glucose-responsive insulin secretion and expressing key β cell functional transcripts by the end of the 27-day differentiation process. We observed a modest 3.9–6.1-fold increase in secretion in S6w1 clusters when transitioning from 0.1 L to the scaled-up 0.5 L size under both dynamic and static glucose-responsive insulin secretion conditions, compared to primary islets (Fig. 2a–c). Velazco-Cruz and colleagues have shown that SC-islets cultured for 5–7 days tend to secrete low levels of insulin, while prolonged cultures between 9 and 26 days can enhance dynamic maturation for increased insulin secretion, albeit with extensive cell loss[55]. Lower in-vitro insulin release in our S6w1 islets, cultured for 7 days, aligns with previous findings[29,30,55], suggesting an ongoing fetal islet phenotype that may improve following prolonged in-vitro culture (4–6 weeks) and maturation, as demonstrated by Balboa and colleagues[12].

Notably, our S6w1 islets exhibited transcriptomic comparability and enrichment for insulin secretory pathways, glycolysis, and TCA metabolism, along with mature β cell gene transcripts, as reported by Balboa and colleagues[12,34] (Fig. 2d–g). These findings align with numerous previously published and optimized protocols for SC-islet generation, whether in 2D planar[4,11,12,39,54] or combined with suspension cultures[14,16,29,30]. Furthermore, the VW® bioreactor-based cell generation process yielded positive outcomes by preserving cell viability, enhancing islet-IEQ yield, and promoting metabolic, transcriptional, and functional maturation of insulin-producing cells, both in vitro and in vivo. Transplantation of S6w1 cells effectively reversed diabetes rapidly and maintained normoglycemia long-term, demonstrating efficient engraftment and functional maturity of S6w1 cells, providing the ability to regulate glucose fluctuations akin to native islets (Fig. 3b, c). Follow-up examinations at two to 4 months revealed improved glucose tolerance and humanization of mice with human c-peptide, confirming enhanced SC-islet graft function, as previously reported (Fig. 3d–f). Moreover, histological examination of the engrafted tissue and marker-labeled characterization indicated that S6w1 cells survived and underwent in vivo maturation into all endocrine islet cells, along with vascularization and minimal exocrine-ductal tissue formation. The presence of cytokeratin19-positive cells, as labeled in ductal tissue, may suggest the formation of benign microcysts within the grafts (Fig. 3g, h).

All directed differentiation protocols to generate SC-islets deliver similar progression of endocrine fate as seen during embryonic pancreatic development and therefore produce all cell types. The time required for maturation of stem cell-derived islets (particularly SC-β cells) is highly variable and often requires an extended maturation period of 2–4 weeks after Stage-6 to become functionally comparable to adult donor islets. Several preclinical studies reported improved and accelerated maturation of SC-β cells in transplanted SC-islet grafts compared to ex-vivo cultures. In this present study, we also observed similar outcomes in all transplanted animals that showed rapid reversal of hyperglycemia as early as 45 days post transplantation and continued to mature until 16 weeks with an increase in human C-peptide in circulating blood (Fig. 3b). Recent evidence from ongoing clinical trials, including Vertex Pharmaceuticals[9], Shanghai-Hangzhou Reprogenix Bioscience[18], and Hao Yin group[10], also suggests that fully differentiated SC-islets graft may take 3–4 months' time to efficiently engraft, functionally integrate and mature into functional and secretive insulin producing cells in transplanted patients living with diabetes. These findings, collectively, suggest that the in-vivo maturation period may

complement the need for extended functional maturation in-vitro. From a patient's perspective with 30 or more years of diabetes, it may not matter that it takes some months to accrue full functionality. From a cell safety perspective, presumably the most stable end-product implanted will be the safest in term of risk of unchecked growth or off target response.

It is widely recognized that the in vivo microenvironment plays a crucial role in enhancing the functional maturation of transplanted endocrine cells following engraftment[68]. During in vitro differentiation, some cells or populations may stray from the endocrine lineage. The efficacy of a differentiation protocol is evaluated by the homogeneity of the final endocrine product. Uncommitted cells primarily develop into enterochromaffin and ductal populations which may pose a risk of cyst or tumors after transplantation. However, work remains to understand how the microenvironment in vivo, particularly the extracellular matrix and cellular interactions beneath the kidney capsule, influence cell maturation. To investigate this, we conducted a comparative transcriptome analysis of harvested endocrine grafts at 8- and 16-weeks post-transplantation. We observed significant overexpression of key islet maturation genes, including *G6PC2, PCSK1, IAPP, CPE, MAGA, NKX6-1, UCN3, MAFB*, and *ISL1* at 16 weeks compared to pre-transplanted S6w1 cells. Moreover, zinc transporter *SLC30A8, ABCC8*, and alpha cell maturation marker *ARX* were upregulated, while INS transcripts remained unchanged. Additionally, we noted downregulation of SLC18A1 expression in matured graft cells, indicating a progressive commitment to β-cell differentiation and maturation following engraftment, supported by the in-vivo microenvironment (Fig. 3i). Furthermore, single-cell composition analysis of graft tissue using flow cytometry revealed a presence of defined islet cell composition and pancreatic lineage cells, collectively indicating in-vivo endocrine maturation, as previously reported (Fig. 3j)[12,14,68].

Despite displaying a fetal maturation phenotype, analysis of RNA transcriptomic data at the single-cell level, when compared with donor islets, confirmed the absence of a higher degree of cellular heterogeneity. Through comprehensive single-cell RNA sequencing (scRNAseq) analysis and extrapolations of islet cell populations using Azimuth projections from human donor islet datasets, it was clearly demonstrated that our S6w1 cells are comparable and exhibit transcriptomically mature islet cell populations (Fig. 4). Clusters identified in our S6w1 datasets confirmed the presence of subpopulations for β- and α-cell identity, with a low frequency of bimodal expression for INS and GCG transcripts, indicating immaturity and a fetal phenotype compared to adult islets (Fig. 4). Unsupervised projection for pivotal islet developmental genes and off-target transcriptomics evidently suggested that the efficiency of our differentiation method and the utility of bioreactor technology are promising for high-quality SC-islet generation without contaminating off-target cell populations (Fig. 5**;** Supplementary fig. 2).

We conducted a comparison of our transcriptomic datasets from S6w1 clusters against published datasets from two independent SC-islet protocol studies[12,68]. The protocol is capable of generating transcriptionally comparable islet cells, albeit with a modest degree of islet maturity, consistent with the methods described by Balboa et al.[12] and Augsornworawat et al.[68] (Fig. 6). Once again, our S6w1 dataset shows a lower degree of bimodal INS expression and transcripts from several β-cell maturation genes, suggesting that the duration for β-like maturation might be insufficient, and further maturation steps may enhance the functional status of SC-β cells. Further, our observed comparable transcriptomic resolution of S6w1 cells as recently reported by Xiaofeng Huang and colleages[51]. It's important to note, despite maturation differences, our SC-islets achieved efficient functionality and the ability to reverse diabetes, post-transplantation. The in vitro culture and maturation process is costly and labor-intensive. Circumventing this process is highly favorable for GMP manufacturing for clinical application.

Suspension-cultured SC-islets are susceptible to uncontrolled cellular heterogeneity at S4 progenitor and S6 maturation stages. Our method robustly demonstrates a controlled mechanism to minimize such unwanted off-target cellular heterogeneity, focusing specifically on endocrine islet cell populations. Of particular interest is the implication of single-cell mass flow cytometry analysis, which allows for the discernment of SC-islet phenotypes, confirming the presence of proteomic differences in developing cell populations, in addition to genomic architecture and functional efficiency. The levels of cellular maturity achieved at the end of stage-6 align with those of established protocols previously reported[11,12,14]. Dimensionality reduction analysis of S4 and S6 single-cell mass flow cytometry datasets reveals higher efficiency in producing homogeneous pancreatic progenitor cells and phenotypically enriched islet cell populations, without inheriting off-target cellular heterogeneity (Fig. 7). Thus, the utilization of VW® bioreactor technology and modifications based on the work of Sui et al.[39] in our optimized full suspension islet generation method presents a scalable tool for reliably producing human SC-islets from stem cells with controlled and minimal heterogeneity.

In summary, we introduce a scalable full suspension (3D) protocol for the reliable and reproducible manufacturing of functional SC-islets within a 27-day culture period. Our study highlights the efficacy of VW® bioreactors in facilitating the scale-up manufacturing of SC-islets, producing a comparable product to human donor islets. This protocol offers several advantages. Firstly, the bioreactor system allows for precise control of the fluidic microenvironment, including oxygen and nutrient levels, pH, and shear forces, as demonstrated by computational bioengineering studies[60,62]. Secondly, it enables optimal islet differentiation by eliminating the need for multi-vessel pooling and controlling off-target heterogeneity resulting from batch-to-batch variation. Thirdly, with significant IEQ yield, the process can be swiftly translated into clinical-grade, low-cost SC-islet manufacturing to meet patient-required mass in a single batch manufacturing using closed-system cGMP-grade technology. This has the potential to revolutionize the future of cell therapy and the cost-economics of diabetes treatment.

In this study, we devised a full suspension scale-up manufacturing protocol to produce human iPSC-derived islet cells, utilizing VW® bioreactor technology. Our research demonstrates promising advancements in cell manufacturing, quality-controlled process development, and closed-system GMP seed train, aimed at commercializing a clinical-grade islet cell product for diabetes treatment. Future research endeavors will further explore the potential of such bioreactors for automated cell manufacturing, enabling the production of large batches of SC-islets and facilitating cryopreservation for use as a cell therapy product. Ongoing efforts will focus on refining and comparing published protocols to enhance differentiation, safety and maturation for their widespread applicability and functional efficacy.

Methods

Experimental model and subject details

All procedures for human iPSC line generation and protocols have been reviewed and approved by the Stem Cell Oversight Committee (SCOC), Canada and the University of Alberta Institutional Health Research Ethics Board (PRO00084032). This study adhered to the Declaration of Helsinki. All animal protocols were conducted in accordance with the Canadian Council on Animal Care Guidelines and Policies with approval from the Animal Care and Use Committee (Health Sciences) (protocol number-AUP00000331) for the University of Alberta. Euthanasia was performed by filling the euthanasia chamber at a rate of 25% CO_2 chamber volume per minute to cause the least amount of distress to rodents. Patients recruited in this study as blood sample donors provided written consent for use of tissue, cell reprogramming, and result disclosure. All experiments were planned a priori and completed in biological and technical triplicates based on standard experimental procedures without exclusion of experimental groups. Randomization was not performed but throughout experimental procedures the scientist performing analysis was blinded to the group allocation of samples including grafts after recovery.

Cell culture

Cell culture was performed in a Class-II biocontainment compliant lab with cell processing in a complete sterile environment using a biosafety cabinet

with high efficiency particulate air filtration. Cells were maintained at 37 °C with 5% CO_2 within humified incubators.

Generation, maintenance, and expansion of human induced pluripotent stem cell lines

Three human iPSC lines generated from peripheral blood mononuclear cells (PBMCs) from human donors (patient demographics in Supplementary Material Table S1) were used in this study. We generated and tested iPSC lines from three donors to compare and test the performance of our differentiation protocol across heathy and diabetes states. Furthermore, our ultimate goal is to attempt to generate autologous cell products from patients with different forms of diabetes that could be transplanted back without need for chronic immunosuppression. We therefore felt it important to test these protocols in iPSC products derived from patients with these disease states. The rational of using three donor iPSC lines is to test the performance of VW-bioreactors for SC-islets generation with similar efficacy under diseased states. This allowed us to confirm that cells obtained from healthy- non-diabetes, total pancreatectomy diabetes and type-1 diabetes can be produced without major differences. Donor blood (20 mL) was collected in a sterile fashion into BD vacutainer spray coated K2EDTA tubes (Fisher Scientific, cat. 13-680-61) and PBMCs were isolated using density gradient centrifugation on Histopaque and expanded by using StemPro-34 Serum Free Complete Media (Gibco, cat. A14509) supplemented with cytokines (10 ng/mL IL3, IL6, SCF and FLT3: R&D Systems, cat. 203-GMP, 206-IL, 7466-SC, and 308E-GMP respectively) for 4 days to achieve satisfactory cell numbers prior to iPSC reprogramming using Sendai virus. iPSCs were generated using the CytoTune iPS 2.0 Sendai Reprogramming Kit (Thermo Fisher, cat. A16517). Between days 15 and 20, a minimum of 10-12 individual colonies (referred as clones hereafter) were manually isolated by handpicking under 10X phase objective (using ECHO inverted Rebel microscope and ECHO image acquisition application on 10.1in iOS device (ECHO) and subcultured as individual iPSC clonal cell lines. Each cell line was scrutinized for routine pluripotent stem cell quality control criteria (ALP staining, phenotype, genetic analysis, and genomic integrity) as previously described and reported[38]. iPSC lines were cultured on 60-mm rhVTN coated plates in StemFlex media (Stem Cell Technologies, cat. A3349401) and passaged using CTS EDTA Versene Solution (Fisher Scientific, cat. A4239101) supplemented with 2 µl/mL Rho-kinase inhibitor (RockI; Y-27632 Stem Cell Technologies, cat. 72304).

For expansion in Vertical Wheel (VW) Bioreactors, 2×10^6 iPSCs harvested from expanded cells on a 60-mm rhVTN coated plates were adapted to suspension culture in 0.1 L VW Bioreactors (PBS Biotech, cat. FA-0.1-D-001) for a minimum of 3 passages before differentiation. For scale-up purpose, 4th passage onwards cells were harvested and counted as single cells to reseed at a concentration of 40,000/ml (10 million live cells) in 0.5 L vessel (PBS Biotech, cat. no. FA-0.5-D-001). Cells were resuspended in 250 mL of StemFlex media with RockI (2 µL/mL) (day 1) and cultured at a constant rotational speed of 60 rotations per minute (rpm). After 24 h, clustered iPSCs were then supplemented with an additional 250 mL of StemFlex media without RockI. On days 4 clusters were allowed to settle down by gravity for 10 min inside the incubator and the top 250 mL of StemFlex was removed with fresh 250 mL of pre-warmed StemFlex media. On day 6, clusters were ready for differentiation and subjected to stage-1 differentiation. Human iPSC lines characteristics and quality control criteria for pluripotency parameters are listed in Supplementary Material Table S2. Genetic stability of cell lines was tested using genotyping RT-PCR kit (Stem Cell Technologies, cat. 07550) as described in Supplementary Material Table S5.

Differentiation of induced pluripotent stem cell lines

For suspension differentiation, iPSCs were seeded into either 0.1 L or 0.5 L VW bioreactor vessels and base medium supplemented with stage- specific growth factors was changed every alternate day moving from S1 to S6, until day 27. Clusters were differentiated at 37 °C with 5% CO_2 and 60 rpm speed. The differentiation was carried out in a six-stage protocol modified differentiation protocol adopted from previously reported publications[13,39]. Complete media formulations and differentiation schedule for suspension differentiation in each vessel volume are available in the Supplementary Material Table S3. Prior to the media changes, clusters were allowed to settle down with gravity for 5 min and fresh media was replenished every alternate day as per the schedule. For routine quality control, 1000–1500 clusters after each stage were dispersed into single cells using pre-warmed accutase, fixed and stored in Cytofix/Cytoperm (BD Biosciences, catalog no. 554714) at 4 °C.

Isolation of primary adult islets

Human islets were obtained from The Alberta Diabetes Institute Islet Core (University of Alberta, Canada) after donor family research consent, and after Health Research Ethics Board review (Pro00001620). Islet donor characteristics are listed in Supplementary Material Table S4. For transcriptomic comparison, human donor islets and SC-islets datasets were used from published open source- GEO repositories and used in accordance with ethical and institutional guidelines.

Brightfield imaging and dithizone staining

Phase contrast bright field images of 3D iPSCs clusters, differentiating clusters and SC-islets at day 27 were captured under 10X phase objective using ECHO inverted Rebel microscope and ECHO image acquisition application on 10.1in iOS device (ECHO). At the end of Stage-6, handpicked 500-1000 SC-islets were stained with zinc-binding dye- dithizone at 37 °C and 5% CO_2 for 15 min to confirm the presence of stored insulin granules in differentiating islets cells. Deep red crimson color in stained islets clusters depicted confirmation of islet differentiation. Stained clusters were finally imaged under 10X brightfield objective using ECHO inverted Rebel microscope on 10.1in iOS device (ECHO).

Immunohistochemistry and image analysis

SC-islets differentiated in suspension conditions and explanted grafts were fixed overnight in 4% PFA and embedded in paraffin for microtomy sectioning in the core facility at the Alberta Diabetes Institute, University of Alberta, Canada. Sections (5 µm) of both Sc-islets and grafts were deparaffinized and rehydrated and subjected to antigen retrieval using citrate buffer (0.0126 M citric acid, Sigma cat. C-0759; 0.0874 M sodium citrate, Sigma, cat. S-4641; pH 6.0) for a total of 20 min. Coverslips and slides were then blocked and permeabilized with 5% normal donkey serum (Sigma, cat. S30-M) in FoxP3 permeabilization buffer (Biolegend, cat. 421402) for 1 h at room temperature (RT) and incubated with primary antibodies diluted in permeabilization buffer overnight at 4 °C. Secondary antibodies were diluted similarly and incubated for 1 h at RT and DAPI (Sigma, D1306) staining for 4 min at RT was used for nuclear visualization. All antibodies used are listed in Supplementary Material Table S6. Slides were visualized using the Zeiss Observer Z1 inverted fluorescence motorized microscope and images were processed using the Zen2 Blue Edition v.2 (Zeiss) and analyzed using QuPath[69].

Flow cytometry

Pancreatic stage-specific cells (Stage1-5) and SC-islets (S6w1) were dissociated with pre-warmed accutase for 10 min in a 37 °C water bath and resuspended in 1 mL of PBS. Cells were strained through a 40 µm strainer, fixed with 4% PFA for 20 min at RT and permeabilized using Cytofix/Cytoperm (BD Biosciences, catalog no. 554714) for 20 min on ice followed by twice washes with 1x Perm/Wash buffer (BD Biosciences, catalog no. 554714). Primary antibodies were incubated for 1 h on ice, or overnight at 4 °C when required, and secondary antibodies for 30 min according to the dilutions in Supplementary Material Table S6. Cells were resuspended in FACS buffer (2% FCS, 2 mM EDTA in DPBS) prior to acquisition. 50,000 cells per samples were acquired to analyse stage-specific QC parameters on single cells after doublet discrimination. Data were acquired using the CytoFLEX S flow cytometer and analyzed using the CytExpert software (Beckman Coulter), FlowJo v.10 (BD Biosciences) and Cytobank v10.0

premium subscription (Beckman Coulter). Dimensionality reductional analysis was performed using FlowSOM self-organizing map and viSNE analysis packages using Cytobank v10.0[70], which uses machine learning algorithms to cluster cells based on maker expression and allowed visualization for cellular heterogeneity.

RNA extraction and gene expression

Stage-specific cells (Stage 1–5) and SC-islets (S6w1) were lysed with 350 µL RLT buffer (Qiagen, cat. 79216) and frozen at −80 °C until RNA extraction. A 30 mg of grafts were lysed in RLT buffer followed by sonication and frozen at −80 °C until RNA extraction. Suspension of lysed cells or tissues in RLT buffer was defrosted and cells were disrupted and homogenized using the QIAshredder system (Qiagen, cat. 79656) and total RNA was then extracted with the RNeasy Mini Kit (Qiagen, cat. 74104) according to the manufacturer's instructions. Concentration and purity of the isolated RNA samples was evaluated using spectrophotometry with the Multiskan Sky-High Microplate Spectrophotometer and µdrop plate (Thermo Fisher, cat. A51119600DPC) by assessing the 260/280 nm and 260/230 nm absorption of samples. Samples were then stored at −80 °C until needed; RNA was quantified after each defrost. RNA was reverse transcribed using the RevertAid First Strand cDNA Synthesis Kit as per manufacturer guidelines (Thermo Fisher, cat. K1621). Complement DNA (cDNA) was stored at −20 °C until required for PCR. To quantitatively study gene expression, custom designed TaqMan Low Density Array Cards were procured and used as per manufacturer instructions (Fisher Scientific cat. 4342253); gene array set up is described in Supplementary Material Table S7. Briefly, 500 ng of cDNA were combined into a solution with 55 µL of nuclease free water and 55 µL TaqMan Universal PCR Master Mix (Thermo Fisher cat. 4305719). The combined solution was loaded into the gene array cards, centrifuged, and processed using FAST-384 well array program *via* the QuantStudio 12 K Flex Real-Time PCR system as per the manufacture recommendations. Data was then analyzed as above and represented as a heat map and/or $2(-\Delta\Delta CT)$ and/or volcano plots using GrapBio[71] and https://www.bioinformatics.com.cn/en, a free online platforms for data analysis and visualization.

Single cell RNA sequencing, alignment, and matrix generation

Cells from 300IES S6w1 SC-islets were dispersed by incubating with 2 ml of Accutase solution containing RockI (2 µL/mL) for 10 min at 37 °C in a 15 ml Falcon tube. After 10 min, the tube was vortexed, and the suspension was gently pipetted up and down after 1 min until a single-cell suspension was achieved. The dissociation medium was then diluted by adding 12 ml of warm S6 media with RockI (2 µL/mL), and the cells were mixed by gently inverting the tube. The dissociated cells were filtered through a 40 µm strainer (BD) to eliminate cell clumps, followed by centrifugation at 1200 rpm for 2 min. The cells were subsequently washed twice in encapsulation buffer (1 × PBS with 0.04% BSA), counted, and adjusted to a concentration of 1×10^6 cells/ml for encapsulation.

Samples of S6w1 SC-islet Cells were prepared following the protocol of the 10X Genomics Single Cell 3' V3.1 Reagent Kit. They were processed using the 10X Genomic Chromium Controller for partitioning and barcoding, and the cDNA library was generated at the Advanced Cell Exploration Core- University of Alberta. The total cell concentration was assessed using the Countess, followed by sequencing on the NovaSeq 6000 System (Illumina) at the core facility at Centre for Health Genomics and Informatics, University of Calgary. The resulting FASTQ files were aligned using Cell Ranger V.7.0.0 with Single Cell 3' V3 chemistry on the 10X Cloud pipeline. We analyzed 17,393 cells to perform quality control pre-processing and analyzed 12,639-14,270 cells with r = 0.9 between nFeature_RNA and nCount_RNA and <25% mitochondrial DNA content. We used Azimuth v0.3.2; R Studio v2023.12.1 + 402; and Seurat v4.0.0 to project our S6w1 scRNAseq datasets onto a publicly available Azimuth integrated human pancreas reference[42–49] to discover an appropriate alignment of distinct islet cell populations (Fig. 4a). For human donor islet samples, datasets from a published study were utilized. Once the 10X h5 format file was created, data analysis was performed on the R Studio v2023.12.1 + 402; and Seurat v4.0.0.

Quality control, integration, and projection

Gene expression profiles from individual cells were generated utilizing the 10x Genomics Chromium Single-Cell 3′ RNAseq platform, employing the Chromium Next GEM Single-Cell 3′ Gene Expression (v.3 chemistry). A total of 17,393 cells were analyzed, amalgamating sequenced libraries from two S6w1 samples across two distinct batches. This yielded an average of 58,817 reads per cell, with 85.1% fraction read, a mean of 8807 UMI counts per cell, and a median of 3,788 genes per cell. Our analysis incorporated two human donor reference single-cell RNA sequencing datasets: (a) from the adult human pancreas (Azimuth-Satija Lab)[42–49], and (b) isolated adult donor islets from three healthy donors (GEO accession# GSE217837)[50]. The healthy donor islet datasets were adapted from Kang et. al[50]. As per their methods, adult donor islets were provided by Prodo Laboratories and were cultured overnight at destination prior to transcriptomics studies. Raw data (fastq) underwent processing using the 10x Genomics Cell Ranger (v.3) pipeline, mapping reads to human reference genomes (GRCh38). UMI counts underwent filtering with RStudio v2023.06.2 + 561 and Seurat v4.3.2 using packages Seurat disk, Seurat data, and tidy verse[72].

Normalization, scaling, and linear dimensionality reduction, including principal component analysis, were conducted on the filtered counts. Top variable features were identified for each sample and combined for analysis. Integrated principal components (PC) facilitated the construction of uniform manifold approximation and projection (UMAP), cell neighborhood identification *via* shared nearest neighbor, and cell clustering using default Seurat methods. The analysis was iterated with adjusted counts, excluding cells with fewer than 800 UMI counts or 500 expressed genes, as well as those exhibiting an unusually high proportion of mitochondrial reads (>25% of counts). Clustering was performed with a resolution of 0.5, and clusters were reordered by similarity and annotated to cell types using differentially expressed genes corresponding to known markers.

We annotated clusters based on markers expression referenced in the Azimuth human pancreas reference- https://azimuth.hubmapconsortium.org/references/human_pancreas/. Subsequently, UMAP and clustering were reconstructed focusing solely on these cells. Differentially expressed genes among clusters and sample types were identified using the FindMarkers function, dot, violin and volcano plots in Seurat, employing default Seurat packages with a log fold-change threshold of 0.25 and statistical cut-off of adjusted $P < 0.05$. The mature beta cell signature was calculated using previously described[12] marker genes, including INS, G6PC2, HOPX, UCN3, IAPP, CHGB, MAFA, and SIX3. Finally, human in vitro islet datasets were projected onto our integrated single-cell RNAseq dataset for reference.

Unsupervised data analysis

Following data quality control, single-cell RNA sequencing (scRNA-seq) data underwent integration using Loupe Browser v7.0 (10X Genomics) without specifying any method parameters or reference genome. A total of 17,393 barcoded counts were processed and filtered based on UMI threshold. Barcodes with UMI counts below 500, featuring less than 800 counts, and exceeding 16% MtUMI were pre-processed and filtered. Subsequently, 13,442 barcodes were subjected to clustering for cell type identification, determined by normalized gene expression levels with reference to previously published canonical pancreatic cell type genes[12,50,73].

Comparative analysis of SC-islet populations from previous published studies

In order to juxtapose the single-cell (SC)-derived cell populations delineated by Balboa et al.[12] and Augsornworawat et al.[68] with our dataset, we amalgamated our Seurat object with their preprocessed and filtered matrix count. Utilizing the read counts (UMI) and metadata presented in GEO submissions (GSE167880 and GSE139535) as a initial reference, we integrated the datasets using Seurat objects and standardized the expression using default

settings as previously detailed[50]. Differentially expressed genes were discerned independently for each sample and SC- β and SC- α clusters in contrast to our S6w1 dataset employing default settings. The normalized data input was projected onto Uniform Manifold Approximation and Projection (UMAP), and UMAP values were employed to discern neighboring cells using default settings. Clustering was performed with a resolution set to 0.5. Clusters displaying correlation with previously identified cell types[50] were illustrated in dot plots and feature plots. Some clusters were manually annotated, particularly those exhibiting expression of endocrine and nonendocrine cell markers in comparison to our endocrine cell dataset for direct comparison.

Glucose stimulated insulin secretion: Dynamic real time and static tests for glucose stimulated insulin secretion were carried out in 1.5 mL tubes. A total of 30–50 SC-islets were handpicked and equilibrated in Krebs-Ringer buffer (KRB) with 2.8 mM glucose (G3) for 120 min, and then subjected to sequential 30-min incubations of G3, 16.8 mM glucose (G17), and 30 mM KCl in KRB. After the tests, the SC-islets and supernatant were collected, and the insulin and DNA contents were analyzed. Dynamic tests of insulin secretion were carried out using a perifusion apparatus (Brandel Suprafusion SF-06) with a flow rate of 0.1 ml min^{-1}, and sampling every 4 min. A total of 50 handpicked SC-islets were used for each test. The SC-islets were equilibrated in G3 for 120 min prior to sample collection. Insulin content in collected fractions and lysates was analyzed with enzyme-linked immunosorbent assay (ELISA) (Mercodia, cat. 10-1132-01).

Diabetes induction and SC-islet transplantation into SCID-beige mice

Five days prior to transplantation, diabetes was induced by intraperitoneal (IP) injection of 175 mg/kg of streptozotocin (STZ; Sigma-Aldrich, ON, Canada) in acetate buffer, pH 4.5 (Sigma-Aldrich, ON, Canada). Immunocompromised SCID beige mice (10–16-week-old) mice were considered diabetic following a non-fasting blood glucose measurement ≥15.0 mmol/L on two consecutive days. A total of 2500 IEQ SC-islets were separated into tubes corresponding to 1.5 million beta-like cells (C-peptide$^+$Nkx6.1$^+$Isl-1$^+$) and transplanted under the kidney capsule as previously described by Pepper et al.[74]. Institutional guidelines for perioperative care, anesthesia and pain management were followed.

Evaluation of SC-islet graft function

Glycemic control was assessed using non-fasting blood glucose measurements (mmol/L) thrice weekly after transplantation using a portable glucometer (OneTouch Ultra 2, LifeScan, Canada). Diabetes reversal was defined as two consecutive readings <11.1 mmol/L. SC-islet grafts were retrieved by total nephrectomy three and/or 6 months after transplantation. Retrieved grafts were characterized using IHC, flow cytometry and/or RT-qPCR. For IHC, complete or partial grafts were fixed overnight in 4% PFA and embedded in paraffin as previously described. For flow cytometry analysis, grafts were digested with 2 mg/ ml collagenase Type V (Sigma, cat. 9623) for 10 min in a 37 °C water bath with shaking every 2.5 min. Single cells were fixed in PFA for flow cytometry analysis. Lastly, for RT-qPCR, up to 30 mg of graft tissues were stored in RLT buffer, minced, and sonicated prior to and frozen at −80 °C.

Furthermore, glucose tolerance tests were conducted at 8, 12, and 16 weeks after transplant, as a means to assess functional efficacy of graft cells in response to a glucose bolus, mimicking postprandial stimulus. Animals were fasted overnight before receiving an intraperitoneal glucose bolus (3 g/kg). Blood glucose levels were monitored at 0, 15, 30, 60, 90, and 120 min after injection, allowing for area under the curve (AUC)-blood glucose to be calculated and analyzed between transplant groups. C-peptide content at 0 and 60 min after injection were analyzed with enzyme-linked immunosorbent assay (ELISA) (Alpco, cat. 80-CPTHU-CH01).

Data collection and statistical methods

Morphological data represents population-wide observations from 4–8 independent differentiation experiments from three donor iPSC lines. viSNE and FlowSOM dimensional reduction visualization, insulin secretion and transcriptomic data represents samples of independent SC-islet differentiation experiments or islet donors. In vivo data is derived from independent animals. Statistical methods used are represented in each Figure legends. All statistical analysis was performed using one-way analysis of variance (ANOVA), multiple comparison using Turkey correction, unpaired parametric *t*-test, and two-way ANOVA with multiple comparison using Šidák correction with 95% confidence interval. All data are presented as either as median with 25–75 percentile interval or mean ± sem.

Data availability

All data are available in the main text or supplementary materials. All RNA sequencing data are deposited in the Gene Expression Omnibus database under accession code GSE266878. All other data are available upon reasonable request from the corresponding authors.

Received: 22 August 2024; Accepted: 11 April 2025;
Published online: 29 May 2025

References

1. Melton, D. The promise of stem cell-derived islet replacement therapy. *Diabetologia* **64**, 1030–1036 (2021).
2. Ramzy, A. et al. A century-long journey from the discovery of insulin to the implantation of stem cell-derived islets. *Endocr. Rev.* **44**, 222–253 (2023).
3. Shapiro, A. M. J. & Verhoeff, K. A spectacular year for islet and stem cell transplantation. *Nat. Rev. Endocrinol.* **19**, 68–69 (2023).
4. Nair, G. G., Tzanakakis, E. S. & Hebrok, M. Emerging routes to the generation of functional beta-cells for diabetes mellitus cell therapy. *Nat. Rev. Endocrinol.* **16**, 506–518 (2020).
5. Du, Y. et al. Human pluripotent stem-cell-derived islets ameliorate diabetes in non-human primates. *Nat. Med* **28**, 272–282 (2022).
6. Maxwell, K. G. & Millman, J. R. Applications of iPSC-derived beta cells from patients with diabetes. *Cell Rep. Med.* **2**, 100238 (2021).
7. Dadheech, N. et al. Opportunities and impediments of human pluripotent stem cell-derived islets in the treatment of diabetes. *J. Immunol. Regen. Med.* **17**, 100064 (2022).
8. Shapiro, A. M. J. et al. Insulin expression and C-peptide in type 1 diabetes subjects implanted with stem cell-derived pancreatic endoderm cells in an encapsulation device. *Cell Rep. Med.* **2**, 100466 (2021).
9. Incorporated, V. P. Glucose-dependent insulin production and insulin-independence in type 1 diabetes from stem cell–derived, fully differentiated islet cells—updated data from the VX-880 clinical trial. in *83rd Scientific Sessions* (American Diabetes Association, 2023).
10. Wu, J. et al. Treating a type 2 diabetic patient with impaired pancreatic islet function by personalized endoderm stem cell-derived islet tissue. *Cell Discov.* **10**, 45 (2024).
11. Hogrebe, N. J., Maxwell, K. G., Augsornworawat, P. & Millman, J. R. Generation of insulin-producing pancreatic beta cells from multiple human stem cell lines. *Nat. Protoc.* **16**, 4109–4143 (2021).
12. Balboa, D. et al. Functional, metabolic and transcriptional maturation of human pancreatic islets derived from stem cells. *Nat. Biotechnol.* **40**, 1042–1055 (2022).
13. Sui, L., Leibel, R. L. & Egli, D. Pancreatic beta cell differentiation from human pluripotent stem cells. *Curr. Protoc. Hum. Genet* **99**, e68 (2018).
14. Veres, A. et al. Charting cellular identity during human in vitro beta-cell differentiation. *Nature* **569**, 368–373 (2019).
15. Nair, G., Hebrok, M. & Russ, H. Rapid generation of functional mature pancreatic islet-beta cells from human pluripotent stem cells. *Protoc. Exch.* **2/4** (2012).
16. Braam, M. J. S. et al. Protocol development to further differentiate and transition stem cell-derived pancreatic progenitors from a monolayer into endocrine cells in suspension culture. *Sci. Rep.* **13**, 8877 (2023).

17. Ramzy, A., et al. Implanted pluripotent stem-cell-derived pancreatic endoderm cells secrete glucose-responsive C-peptide in patients with type 1 diabetes. *Cell Stem Cell* **28**, 2047–2061.e2045 (2021).
18. Wang, S., et al. Transplantation of chemically induced pluripotent stem-cell-derived islets under abdominal anterior rectus sheath in a type 1 diabetes patient. *Cell* **187**, 6152–6164.e6118 (2024).
19. Marfil-Garza, B. A. et al. Pancreatic islet transplantation in type 1 diabetes: 20-year experience from a single-centre cohort in Canada. *Lancet Diabetes Endocrinol.* **10**, 519–532 (2022).
20. Pellegrini, S., Zamarian, V. & Sordi, V. Strategies to improve the safety of iPSC-derived beta cells for beta cell replacement in diabetes. *Transpl. Int* **35**, 10575 (2022).
21. Bogacheva, M. S. et al. Differentiation of human pluripotent stem cells into definitive endoderm cells in various flexible three-dimensional cell culture systems: possibilities and limitations. *Front. Cell Dev. Biol.* **9**, 726499 (2021).
22. Diekmann, U. et al. Chemically defined and xenogeneic-free differentiation of human pluripotent stem cells into definitive endoderm in 3D culture. *Sci. Rep.* **9**, 996 (2019).
23. Aghazadeh, Y. et al. GP2-enriched pancreatic progenitors give rise to functional beta cells in vivo and eliminate the risk of teratoma formation. *Stem Cell Rep.* **17**, 964–978 (2022).
24. Cuesta-Gomez, N. et al. AT7867 promotes pancreatic progenitor differentiation of human iPSCs. *Stem Cell Rep.* **14**, 2084–2095 (2023).
25. Nair, G. G. et al. Recapitulating endocrine cell clustering in culture promotes maturation of human stem-cell-derived beta cells. *Nat. Cell Biol.* **21**, 263–274 (2019).
26. Iworima, D. G., Rieck, S. & Kieffer, T. J. Process parameter development for the scaled generation of stem cell-derived pancreatic endocrine cells. *Stem Cells Transl. Med.* **10**, 1459–1469 (2021).
27. Iworima, D. G. et al. Metabolic switching, growth kinetics and cell yields in the scalable manufacture of stem cell-derived insulin-producing cells. *Stem Cell Res. Ther.* **15**, 1 (2024).
28. Hogrebe, N. J., Augsornworawat, P., Maxwell, K. G., Velazco-Cruz, L. & Millman, J. R. Targeting the cytoskeleton to direct pancreatic differentiation of human pluripotent stem cells. *Nat. Biotechnol.* **38**, 460–470 (2020).
29. Pagliuca, F. W. et al. Generation of functional human pancreatic beta cells in vitro. *Cell* **159**, 428–439 (2014).
30. Pollock, S. D., Galicia-Silva, I. M., Liu, M., Gruskin, Z. L. & Alvarez-Dominguez, J. R. Scalable generation of 3D pancreatic islet organoids from human pluripotent stem cells in suspension bioreactors. *STAR Protoc.* **4**, 102580 (2023).
31. Abdulreda, M. H. & Berggren, P. O. Challenges in stem cell-derived islet replacement therapy can be overcome. *Cell Transpl.* **30**, 9636897211045320 (2021).
32. Kelly, O. G. et al. Cell-surface markers for the isolation of pancreatic cell types derived from human embryonic stem cells. *Nat. Biotechnol.* **29**, 750–756 (2011).
33. Stock, A. A. et al. Conformal coating of stem cell-derived islets for beta cell replacement in type 1 diabetes. *Stem Cell Rep.* **14**, 91–104 (2020).
34. Schmidt, M. D., Ishahak, M., Augsornworawat, P. & Millman, J. R. Comparative and integrative single cell analysis reveals new insights into the transcriptional immaturity of stem cell-derived beta cells. *BMC Genom.* **25**, 105 (2024).
35. Hiyoshi, H. et al. Characterization and reduction of non-endocrine cells accompanying islet-like endocrine cells differentiated from human iPSC. *Sci. Rep.* **12**, 4740 (2022).
36. Jensen, N. K. et al. Characterization of the nonendocrine cell populations in human embryonic stem cell-derived (hESC) islet-like clusters posttransplantation. *Toxicol. Pathol.* **49**, 1269–1287 (2021).
37. Cuesta-Gomez, N. et al. Characterization of stem-cell-derived islets during differentiation and after implantation. *Cell Rep.* **40**, 111238 (2022).
38. Cuesta-Gomez, N. et al. Suspension culture improves iPSC expansion and pluripotency phenotype. *Stem Cell Res. Ther.* **14**, 154 (2023).
39. Sui, L. et al. Reduced replication fork speed promotes pancreatic endocrine differentiation and controls graft size. *JCI Insight* **6**, e141553 (2021).
40. Huang, H. H., Harrington, S. & Stehno-Bittel, L. The flaws and future of islet volume measurements. *Cell Transpl.* **27**, 1017–1026 (2018).
41. Cogger, K. F. et al. Glycoprotein 2 is a specific cell surface marker of human pancreatic progenitors. *Nat. Commun.* **8**, 331 (2017).
42. Baron, M., et al. A single-cell transcriptomic map of the human and mouse pancreas reveals inter- and intra-cell population structure. *Cell Syst.* **3**, 346–360.e344 (2016).
43. Grun, D. et al. De novo prediction of stem cell identity using single-cell transcriptome data. *Cell Stem Cell* **19**, 266–277 (2016).
44. Hao, Y., et al. Integrated analysis of multimodal single-cell data. *Cell* **184**, 3573–3587.e3529 (2021).
45. Lawlor, N. et al. Single-cell transcriptomes identify human islet cell signatures and reveal cell-type-specific expression changes in type 2 diabetes. *Genome Res.* **27**, 208–222 (2017).
46. Muraro, M. J. et al. A single-cell transcriptome atlas of the human pancreas. *Cell Syst.* **3**, 385–394 e383 (2016).
47. Segerstolpe, A. et al. Single-cell transcriptome profiling of human pancreatic islets in health and type 2 diabetes. *Cell Metab.* **24**, 593–607 (2016).
48. Stuart, T., et al. Comprehensive integration of single-cell data. *Cell* **177**, 1888–1902.e1821 (2019).
49. Xin, Y. et al. Single-cell RNA sequencing and analysis of human pancreatic islets. *J. Vis. Exp.* **18**, https://doi.org/10.3791/59866 (2019).
50. Kang, R. B. et al. Single-nucleus RNA sequencing of human pancreatic islets identifies novel gene sets and distinguishes beta-cell subpopulations with dynamic transcriptome profiles. *Genome Med* **15**, 30 (2023).
51. Huang, X. et al. Stomach-derived human insulin-secreting organoids restore glucose homeostasis. *Nat. Cell Biol.* **25**, 778–786 (2023).
52. Pullen, T. J. et al. Identification of genes selectively disallowed in the pancreatic islet. *Islets* **2**, 89–95 (2010).
53. Martens, G. A. et al. Clusters of conserved beta cell marker genes for assessment of beta cell phenotype. *PLoS ONE* **6**, e24134 (2011).
54. Rezania, A. et al. Reversal of diabetes with insulin-producing cells derived in vitro from human pluripotent stem cells. *Nat. Biotechnol.* **32**, 1121–1133 (2014).
55. Velazco-Cruz, L. et al. Acquisition of dynamic function in human stem cell-derived beta cells. *Stem Cell Rep.* **12**, 351–365 (2019).
56. Augsornworawat, P., Maxwell, K. G., Velazco-Cruz, L. & Millman, J. R. Single-cell transcriptome profiling reveals beta cell maturation in stem cell-derived islets after transplantation. *Cell Rep.* **32**, 108067 (2020).
57. Bendall, S. C. et al. Single-cell mass cytometry of differential immune and drug responses across a human hematopoietic continuum. *Science* **332**, 687–696 (2011).
58. Bodenmiller, B. et al. Multiplexed mass cytometry profiling of cellular states perturbed by small-molecule regulators. *Nat. Biotechnol.* **30**, 858–867 (2012).
59. Verhoeff, K. et al. Scalable bioreactor-based suspension approach to generate stem cell-derived islets from healthy donor-derived iPSCs. *Transplantation* **109**, e22–e35 (2024).
60. Lee, B. et al. Cell culture process scale-up challenges for commercial-scale manufacturing of allogeneic pluripotent stem cell products. *Bioengineering (Basel)* **9**, 92 (2022).
61. Borys, B. S. et al. Overcoming bioprocess bottlenecks in the large-scale expansion of high-quality hiPSC aggregates in vertical-wheel stirred suspension bioreactors. *Stem Cell Res. Ther.* **12**, 55 (2021).
62. Borys, B. S. et al. Optimized serial expansion of human induced pluripotent stem cells using low-density inoculation to generate

clinically relevant quantities in vertical-wheel bioreactors. *Stem Cells Transl. Med.* **9**, 1036–1052 (2020).
63. Barsby, T. et al. Differentiating functional human islet-like aggregates from pluripotent stem cells. *STAR Protoc.* **3**, 101711 (2022).
64. Snyder, R. D. & Regan, J. D. Aphidicolin inhibits repair of DNA in UV-irradiated human fibroblasts. *Biochem. Biophys. Res. Commun.* **99**, 1088–1094 (1981).
65. Starczewska, E. et al. Targeting DNA repair with aphidicolin sensitizes primary chronic lymphocytic leukemia cells to purine analogs. *Oncotarget* **7**, 38367–38379 (2016).
66. Waters, R. Aphidicolin: an inhibitor of DNA repair in human fibroblasts. *Carcinogenesis* **2**, 795–797 (1981).
67. Sakuma, K. et al. CDK8/19 inhibition plays an important role in pancreatic beta-cell induction from human iPSCs. *Stem Cell Res. Ther.* **14**, 1 (2023).
68. Augsornworawat, P., Maxwell, K. G., Velazco-Cruz, L. & Millman, J. R. Single-cell transcriptome profiling reveals beta cell maturation in stem cell-derived islets after transplantation. *Cell Rep.* **34**, 108850 (2021).
69. Bankhead, P. et al. QuPath: open source software for digital pathology image analysis. *Sci. Rep.* **7**, 16878 (2017).
70. Kotecha, N., Krutzik, P. O. & Irish, J. M. Web-based analysis and publication of flow cytometry experiments. *Curr. Protoc. Cytom.* **10**, 17 (2010).
71. Zhao, T. & Wang, Z. GraphBio: a shiny web app to easily perform popular visualization analysis for omics data. *Front. Genet.* **13**, 957317 (2022).
72. Butler, A., Hoffman, P., Smibert, P., Papalexi, E. & Satija, R. Integrating single-cell transcriptomic data across different conditions, technologies, and species. *Nat. Biotechnol.* **36**, 411–420 (2018).
73. Augsornworawat, P. et al. Single-nucleus multi-omics of human stem cell-derived islets identifies deficiencies in lineage specification. *Nat. Cell Biol.* **25**, 904–916 (2023).
74. Pepper, A. R. et al. A prevascularized subcutaneous device-less site for islet and cellular transplantation. *Nat. Biotechnol.* **33**, 518–523 (2015).

Acknowledgements

A.M.J.S. is supported through a Canada Research Chair (Tier 1) in Regenerative Medicine and Transplant Surgery, and through grant support from the Canadian Stem Cell Network, Canadian Institute of Health Research, Juvenile Diabetes Research Foundation, Diabetes Canada, Canadian Donation and Transplant Research Program (CDTRP), Alberta Diabetes Foundation and Diabetes Research Institute Foundation of Canada (DRIFCan). B.M.G. is supported by the CHRISTUS Excellence and Innovation Center. We thank Dr. Jean Buteau for providing access to Olympus slide scanning imaging station. We also thank 10X Genomics, USA for their technical support in generating scRNAseq pipeline and data analysis. We would like to extend our heartfelt gratitude to Dr. George Harb, whose insightful guidance and expertise greatly contributed to the conceptualization, methodology, and analysis throughout this research. Their unwavering support and constructive feedback were invaluable in shaping the direction of this study. A.M.J.S. is supported through a Canada Research Chair (Tier 1) in Regenerative Medicine and Transplant Surgery, and through grant support from the Canadian Institute of Health Research, Juvenile Diabetes Research Foundation, Diabetes Canada, Canadian Donation and Transplant Research Project, Diabetes Research Institute Foundation of Canada (DRIFCan), Alberta Diabetes Foundation, and Canadian Stem Cell Network. B.M.G. is supported by the Patronato del Instituto Nacional de Ciencias Medicas y Nutricion Salvador Zubiran (INCMNSZ), the Fundacion para la Salud y la Educacion Dr. Salvador Zubirán (FunSaEd), and the CHRISTUS Excellence and Innovation Center. N.C.G. is supported by the Natural Sciences and Engineering Research Council-Collaborative Research and Training Experience (NSERC-CREATE) program and Juvenile Diabetes Research Foundation Canada as well as the Canadian Institutes of Health Research (MFE—193943).

Author contributions

Following authors have contributed to the preparation of this research article. Conceptualization: N.D., M.B.L., A.M.J.S. Methodology: N.D., M.B.L., Z.P.C., R.P., P.M.D., G.J., A.S., N.R., D.O.'G. Investigation: N.D., M.B.L., Z.P.C., N.C.G., I.T.J., R.P., B.M.G., K.V., S.S., H.R., P.A., J.L. Visualization: N.D., M.B.L., Z.P.C., N.C.G., P.M.D., A.S., A.M.J.S. Funding acquisition: N.D., A.M.J.S. Project administration: N.D., R.P., A.M.J.S. Supervision: N.D., A.M.JS. Writing—original draft: N.D., Z.P.C., N.C.G., A.M.J.S. Writing—review & editing: N.D., Z.P.C., R.P., A.M.J.S.

Competing interests

A.M.J.S. serves as a consultant to Vertex Pharmaceuticals Inc., Betalin Therapeutics Ltd and Aspect Biosystems Inc.

Additional information

Supplementary information The online version contains supplementary material available at https://doi.org/10.1038/s41536-025-00409-y.

Correspondence and requests for materials should be addressed to Nidheesh Dadheech or A. M. James Shapiro.